JGR Biogeosciences

RESEARCH ARTICLE
10.1029/2018JG004776

Iron (Oxyhydr)Oxides Serve as Phosphate Traps in Tundra and Boreal Peat Soils

Elizabeth M. Herndon[1], Lauren Kinsman-Costello[2], Kiersten A. Duroe[1], Jonathan Mills[1], Evan S. Kane[3], Stephen D. Sebestyen[4], Aaron A. Thompson[5], and Stan D. Wullschleger[6]

[1]Department of Geology, Kent State University, Kent, OH, USA, [2]Department of Biological Sciences, Kent State University, Kent, OH, USA, [3]School of Forest Resources and Environmental Science, Michigan Technical University, Houghton, MI, USA, [4]USDA Forest Service, Northern Research Station, Grand Rapids, MN, USA, [5]Crop and Soil Sciences, University of Georgia, Athens, GA, USA, [6]Environmental Sciences Division, Oak Ridge National Laboratory, Oak Ridge, TN, USA

Abstract Arctic and boreal ecosystems are experiencing pronounced warming that is accelerating decomposition of soil organic matter and releasing greenhouse gases to the atmosphere. Future carbon storage in these ecosystems depends on the balance between microbial decomposition and primary production, both of which can be regulated by nutrients such as phosphorus. Phosphorus cycling in tundra and boreal regions is often assumed to occur through biological pathways with little interaction with soil minerals; that is, phosphate released from organic molecules is rapidly assimilated by plants or microorganisms. In contrast to this prevailing conceptual model, we use sequential extractions and spectroscopic techniques to demonstrate that iron (oxyhydr)oxides sequester approximately half of soil phosphate in organic soils from four arctic and boreal sites. Iron (III) (oxyhydr)oxides accumulated in shallow soils of low-lying, saturated areas where circumneutral pH and the presence of a redox interface promoted iron oxidation and hydrolysis. Soils enriched in short-range ordered iron oxyhydroxides, which are susceptible to dissolution under anoxic conditions, had high phosphate sorption capacities and maintained low concentrations of soluble phosphate relative to soils containing mostly organic-bound iron or crystalline iron oxides. Thus, substantial quantities of phosphorus in these organic soils were associated with minerals that could reduce bioavailability but potentially also serve as phosphorus sources under anoxic conditions. The implication of this finding is that mineral surfaces effectively compete with biological processes for phosphate and must be considered as a nutrient regulator in these sensitive ecosystems.

Plain Language Summary The ability of plants to derive nutrients from the soil influences their capacity to photosynthesize and draw carbon out of the atmosphere. Plants compete for nutrients such as phosphate with soil microorganisms and with soil minerals. Iron oxides, in particular, effectively bind phosphate and keep it sequestered from plants. We demonstrate that iron oxides bind high quantities of phosphate in arctic and boreal systems where minerals are often assumed to have negligible influence on biological processes. Although plant biomass is likely to increase in a climate that is warmer and enriched in carbon dioxide, iron oxides may increasingly limit phosphate availability to plants and constrain ecosystem productivity.

Key Points:
- Organic soils contained pH-dependent mixtures of organic-bound iron and iron (oxyhydr)oxides, the latter accumulating in low-lying areas
- Soils enriched in iron (oxyhydr) oxides had high phosphate sorption capacities and low concentrations of water-soluble phosphate
- Nearly half of soil phosphate, representing a quarter of soil phosphorus, was bound to oxide minerals

Supporting Information:
- Supporting Information S1

Correspondence to:
E. M. Herndon,
eherndo1@kent.edu

Citation:
Herndon, E. M., Kinsman-Costello, L., Duroe, K. A., Mills, J., Kane, E. S., Sebestyen, S. D., et al. (2019). Iron (oxyhydr)oxides serve as phosphate traps in tundra and boreal peat soils. *Journal of Geophysical Research: Biogeosciences*, *124*, 227–246. https://doi.org/10.1029/2018JG004776

Received 29 AUG 2018
Accepted 6 JAN 2019
Accepted article online 15 JAN 2019
Published online 7 FEB 2019

Author Contributions:
Conceptualization: Elizabeth M. Herndon, Lauren Kinsman-Costello
Data curation: Kiersten A. Duroe, Jonathan Mills, Aaron A. Thompson
Formal analysis: Elizabeth M. Herndon, Lauren Kinsman-Costello, Kiersten A. Duroe, Jonathan Mills, Aaron A. Thompson
Funding acquisition: Elizabeth M. Herndon
Investigation: Kiersten A. Duroe, Jonathan Mills
Methodology: Elizabeth M. Herndon, Lauren Kinsman-Costello
Resources: Evan S. Kane, Stephen D. Sebestyen, Stan D. Wullschleger
Writing - original draft: Elizabeth M. Herndon, Kiersten A. Duroe, Aaron A. Thompson
(continued)

1. Introduction

Temperatures at northern high latitudes are increasing at twice the global average rate and driving pronounced environmental change (Bekryaev et al., 2010; Hinzman et al., 2013; Stocker et al., 2013). Organic matter that has been stored in soils for centuries to millennia is decomposing more rapidly and releasing excess greenhouse gases to the atmosphere (Oechel et al., 1993; Schuur et al., 2009), and carbon release from thawing permafrost alone could increase global temperatures 8% by 2100 (Schaefer et al., 2014). Increases in plant biomass could partially offset soil C losses (Koven et al., 2011; McGuire et al., 2018; Schuur et al., 2009), but growth may be constrained by nutrient availability (Mekonnen et al., 2018; Wieder et al., 2015). Controls on nutrient limitation, and in particular phosphorus (P) limitation, are not well represented in climate models and remain a major knowledge gap for tundra and boreal ecosystems. In order to predict terrestrial carbon storage in a warmer climate, it is necessary to evaluate the processes that enhance or restrict nutrient bioavailability in these regions.

Writing – review & editing: Elizabeth M. Herndon, Lauren Kinsman-Costello, Evan S. Kane, Stephen D. Sebestyen, Aaron A. Thompson, Stan D. Wullschleger

In particular, changing hydrologic regimes will drive redox shifts that affect nutrient availability. Widespread soil drying is predicted for tundra and boreal ecosystems due to both increases in evapotranspiration and drainage resulting from permafrost thaw (Avis et al., 2011; Bring et al., 2016; Yoshikawa & Hinzman, 2003). Pockets of increased soil saturation are predicted in areas that collapse and fill with water or are recharged by groundwater (Swindles et al., 2016). Transitions between saturated and drained soils affect P bioavailability through its interactions with iron (Fe). In poorly drained, organic-rich soils, such as those that are prevalent in northern peatlands, Fe^{2+} that is leached from soil minerals can migrate to oxic zones (Fiedler et al., 2004; Herndon et al., 2015) and accumulate as a mixture of organic-bound Fe^{II}, organic-bound Fe^{III}, and Fe^{III} (oxyhydr)oxides (Bhattacharyya et al., 2018; Riedel et al., 2013; Sundman et al., 2014). Iron (oxyhydr)oxides, referring here to a suite of iron (III) oxide and oxyhydroxide minerals, are well known to bind phosphate and limit its bioavailability in temperate and tropical systems (Vitousek et al., 2010; Walker & Syers, 1976). Short-range ordered (SRO) iron oxyhydroxides, commonly described as poorly crystalline, can adsorb particularly large quantities of phosphate but are susceptible to reductive dissolution that releases phosphate into solution under anoxic conditions (Chen et al., 2018; Henderson et al., 2012; Kinsman-Costello et al., 2014; Zak et al., 2004). Organically complexed Fe^{III} is also thought to bind phosphate by forming organic-Fe-PO_4 ternary complexes (Kizewski et al., 2010). Although Fe is increasingly reported to accumulate at redox interfaces (Emerson et al., 2015; Giesler et al., 2005; Herndon et al., 2015; Vincent et al., 2014) and influence C cycling in these regions (Lipson et al., 2010; Page et al., 2013; Roy Chowdhury et al., 2015; Trusiak et al., 2018), the abundance and speciation of various iron species in these soils and their abilities to trap phosphate remain unknown.

The importance of P availability in controlling ecosystem carbon balance in certain areas of northern high latitudes, either directly or by modulating N effects, has been repeatedly demonstrated in fertilization studies (Mack et al., 2004; Shaver et al., 1998; Street et al., 2017). Although plant growth will increase rapidly in response to a warming climate and generate a high P demand, weathering of phosphate minerals will remain slow (Chapin et al., 1978), and P availability will be constrained by OM degradation and P sorption/desorption processes in the soil before climate-enhanced mineral weathering could supply additional P to the ecosystem. Phosphorus bioavailability at northern high latitudes is currently thought to be controlled by gradual enzymatic release from soil organic matter (Chapin et al., 1978; Walbridge & Navaratnam, 2006; Weintraub, 2011). Low soluble phosphate concentrations and rapid uptake of added phosphate are typically attributed to high biotic need driving rapid microbial and plant uptake rather than abiotic sorption (Giblin et al., 1991; Harms & Ludwig, 2016; Hill et al., 2014). Oxide-bound P—typically measured after air-drying soils, which may change Fe-P associations—has been assumed to be permanently fixed and isolated from ecosystem processes (Chapin et al., 1978; Giblin et al., 1991). In this study, we demonstrate that iron minerals must also be considered as important regulators of nutrient availability in these systems.

2. Materials and Methods

2.1. Site Description and Soil Sampling

Soils were collected from four long-term observatories that span arctic and boreal ecotones in North America (Figure 1). Within each site, surface soils (<20 cm) were obtained from plots of contrasting saturation. Details regarding each site and sample collection are described below.

The Barrow Environmental Observatory (BEO) is located in the arctic tundra on the coastal plain outside of Utqiagvik, Alaska. Annual precipitation averages 12 cm, and average annual air temperature is −12 °C. The region is underlain by continuous permafrost that restricts drainage and creates a landscape dominated by lakes and interlake polygonal ground (Hubbard et al., 2013). Ice wedge polygons generate microtopographic features that regulate hydrologic flow paths and redox gradients (Lipson et al., 2012; Newman et al., 2015; Zona et al., 2011). Low-centered polygons (LCPs) consist of a sunken center basin bordered by elevated ridges and low-lying troughs, and high-centered polygons (HCPs) consist of an elevated center mound surrounded by low-lying troughs. Three intact soil cores from each feature of a LCP and HCP were collected on 15 October 2015 using a slide hammer equipped with a split soil core sampler (AMS, Inc.). Core depths (12.0 to 29.5 cm) were reported from the surface of the soil to the maximum sampling depth. Each core was wrapped in Al foil, sealed in a plastic bag, and temporarily stored in a −30 °C walk-in freezer at the Barrow Arctic Research Center.

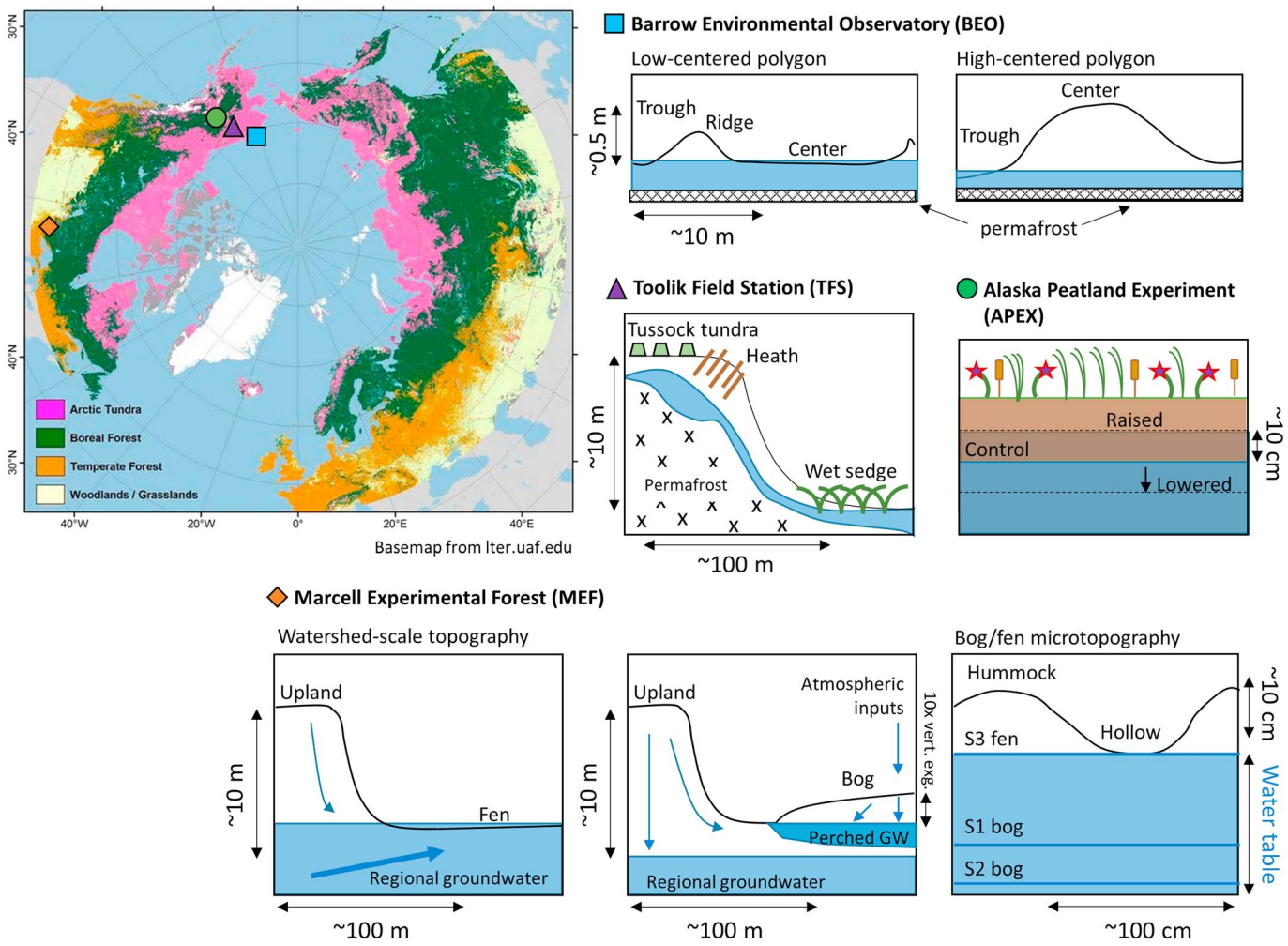

Figure 1. Locations of each site marked on a circumpolar map showing the distribution of arctic tundra and boreal forest (basemap obtained from lter.uaf.edu). Sites include the Barrow Environmental Observatory (blue square), Toolik Field Station/Arctic LTER (purple triangle), Alaska Peatland Experiment (green circle), and Marcell Experimental Forest (orange diamond). Diagrams on the right show different topographic features for each plot within each site, as described in the methods. Length scales are approximate to the nearest order of magnitude. Blue overlays indicate the approximate position of the water table. For the MEF fen, water inputs are dominated by regional groundwater (big arrow) with lesser contributions from upland regions (little arrow). For the MEF bogs, water inputs are predominately sourced from atmospheric inputs, and the bog water is hydrologically isolated from the regional groundwater table. Water table height at APEX represents the average conditions for dry years since water table manipulation began. Water table height at MEF represents conditions observed at the time of sampling. Diagrams were adapted from data or figures reported by previous publications (Giblin et al., 1991; Hubbard et al., 2013; Olefeldt et al., 2017; Verry et al., 2011).

Toolik Field Station (TFS) is a part of the Arctic Long-Term Ecological Research (LTER) site located around Toolik Lake on the Alaskan North Slope at the foothills of the Brooks Range, Alaska, USA. The Toolik region experiences a mean annual air temperature of about −8.5 °C with ~30 cm of precipitation, 40% of which falls during the winter months (Cherry et al., 2014). The landscape is underlain by continuous permafrost with depth of ~200 m, and < 50 cm of the soil surface thaws annually. Surface organic horizon soils were collected to <15-cm depth on 21 July 2015 from near Toolik Field Station on land surfaces developed since the Itkillik I glaciation (>55,000 years ago). Land surfaces glaciated by Itkillik I host soils that are generally acidic (pH < 5.5) and depleted in base cations such as calcium (Whittinghill & Hobbie, 2011). Triplicate soils were collected from topographic positions near but not in LTER fertilization plots that included mesic tussock tundra in the uplands, a relatively dry hilltop heath, and low-lying wet sedge tundra. The tussock tundra is characterized by ~17–25-cm-thick organic horizons with a maximum thaw depth of 30–50 cm (Shaver et al., 2014). The well-drained, deeply thawed (>1-m depth) heath zone contains a thin organic horizon overlying mineral soil. Wet sedge tundra contains ~50-cm-thick organic soils that do not thaw to the mineral

layer (Shaver et al., 2014). The toposequence shown in Figure 1 represents the typical distribution of these features across landscape position in the Toolik region but does not specifically reflect the sampled locations (Giblin et al., 1991; Shaver et al., 2014).

The Alaska Peatland Experiment (APEX) is positioned in a boreal forest ecosystem located about 35 km southeast of Fairbanks, AK, in interior Alaska. Mean annual temperature is −2.9 °C, and mean annual precipitation is 26.9 cm, 30% of which falls as snow (Hinzman et al., 2006; Viereck et al., 1993). The APEX site is a moderate rich fen located within the Tanana River floodplain where greenhouse gas emissions are monitored as a function of hydrology and soil warming (Turetsky et al., 2008). The site lacks microtopography, and maximum peat depth is approximately 1 m. Water table levels are manipulated in two large experimental plots (20 × 20 m) within the fen by either pumping water into the plot to raise the water table or draining water out of the plot to lower the water table. Following initial construction in 2005, ~10-cm average increases and decreases in water table height were observed for raised and lowered plots, respectively, relative to the control, but only during dry years (water table >20 cm below the peat surface; Kane et al., 2010; Olefeldt et al., 2017). Flooding conditions in wet years, including during the time of sampling for this study, have periodically resulted in uniformly high water tables above the soil surface for all plots (Olefeldt et al., 2017). Three replicate soil cores were collected from each treatment plot in late July 2016. Soil cores were extracted using a 1″ diameter drill-powered auger and collected from the base of the living vegetation down to the point of refusal, which ranged between 55.5 and 64 cm. Refusal occurred when the peat soil became compacted. The auger was removed from the peat, and the core was extracted onto aluminum foil where it was then gently stretched by hand to offset compaction that occurred during coring. Soil water content was likely lower than field conditions due to loss of pore water from the saturated soils during extraction. The core was wrapped in aluminum foil, placed into plastic storage bags with excess air removed, and stored frozen until processing.

The Marcell Experimental Forest (MEF) is an 1,140-ha research area that sits at the southern margin of a boreal peatland forest biome in Northern Minnesota, about 40 km north of the Grand Rapids, MN. Annual precipitation averages 78 cm with one third falling as snow. The mean annual temperature since 1961 was 3.4 °C with monthly average temperatures between 16 °C and 19 °C in June, July, and August and between −11 °C and −15 °C in December, January, and February (Sebestyen et al., 2011). The MEF contains six experimental watersheds (five bogs and one fen), each consisting of an upland portion and low-lying peatland with at least one outlet stream that drains a watershed (Sebestyen et al., 2011). Upland runoff from hillslopes with mineral soils drains into fringe areas (laggs) that surround the central bogs (Sebestyen et al., 2011; Verry et al., 2011). Bogs have raised-dome profiles with hollows that rise up to 10–15 cm in elevation above that of laggs (Richardson et al., 2010). These subtle elevation and hydraulic gradients result in bogs that are hydrologically isolated from upland runoff and groundwater inputs from regional-scale aquifers, leaving precipitation and atmospheric deposition as sole sources of water and exogenous solutes. In contrast, fens are areas with throughflow or discharge of aquifer water. The aquifer-water subsidies to fens result in less intra-annual variation in water table fluctuations and greater inputs of minerotrophic waters to fens than bogs.

Eighteen surface soils were collected from the peatlands of watersheds S1 (bog), S2 (bog), and S3 (fen) on 15 October 2015. The S1 bog is a black spruce (*Picea mariana*)—tamarak (*Larix laricina*)—*Sphagnum* raised-dome bog where the Spruce and Peatland Responses Under Climatic and Environmental Change Experiment site is occurring (Hanson et al., 2017). Samples were collected near the outlet stream outside of the Spruce and Peatland Responses Under Climatic and Environmental Change Experiment plots. Over a five-decade-long record, water levels were more variable at the S1 bog than the other peatlands, fluctuating from several centimeters above the peat surface in hollows to a maximum depth of 1.4 m during the most severe drought (Sebestyen et al., 2011). Like other MEF bogs, water tables fluctuate <0.3 m during most years, with deeper drawdown only during prolonged periods with no rainfall. At the time of sampling, the water table was within 15 cm of the hollow surface at bog S1. The S2 bog is a black spruce-*Sphagnum* bog (raised-dome) that includes a minor component of tamarack, especially where cores were collected. The water table in S2 was more than 20 cm below the hollow surface at the time of sampling. The water table at the S3 fen is rarely >15 cm beneath hollow surfaces, and the water table was at the hollow surface at the time of sampling. Triplicate samples were collected from hummock and hollow microtopographic features within each wetland. Hummocks are typically elevated and dry relative to depressed and saturated

hollows. Soils were collected within about a 1 × 1-m area using a 7.5-cm stainless steel drill corer to cut soil from the base of living vegetation to ~20-cm depth. A knife was used to cut around the corer when drilling began to create a cleaner coring at the surface.

2.2. Soil Processing and Characterization

All soils were immediately sealed in plastic bags and frozen upon collection, shipped to Kent State University in coolers with blue ice or dry ice, and stored at −20 °C until processing. Frozen soil cores and bulk surface soils were thawed and processed in a vinyl anaerobic chamber with N_2 atmosphere containing at least 1.0% H_2 and less than 1-ppm O_2. Large roots and other green vegetation were removed from the soils before processing. MEF and TFS surface soils were thawed in the anaerobic chamber, homogenized, and divided into subsamples for physical and chemical characterization (described below). BEO cores were split into an upper organic horizon and a lower mineral horizon using a multipurpose oscillating power tool. The APEX cores ($n = 9$) were split into two sections: <20- and >20-cm depth. This depth corresponds to the approximate depth of peat that experiences seasonal water table variation, although the extent and variability of water table fluctuations varied amongst plots (Kane et al., 2010). A small portion of each horizon was air dried in the anaerobic chamber, lightly ground with a mortar and pestle, and then stored in plastic sample bags in the anaerobic chamber. The remaining wet soil was partitioned into subsamples for physical and chemical characterization.

Soil properties are reported as the mean ± standard error of the mean for values measured on three replicate soils from each plot. Soil pH was measured on a 1:5 ratio of soil mixed with 1-M potassium chloride (KCl) solution in the anaerobic chamber. The 1-M KCl solution was boiled under N_2 gas to remove dissolved O_2 gas prior to use. Soil gravimetric water content was determined as mass loss of the triplicate subsamples following oven drying at 105 °C for 24 hr (Gardner, 1986). Volumetric water content (g H_2O cm^{-3}) was calculated as the product of gravimetric water content (g H_2O g-$soil^{-1}$) and soil bulk density (g-soil cm^{-3}). Soil bulk density was estimated using the relationship between soil organic C and bulk density reported by Bockheim et al. (2003) for soils in the Barrow region. Loss-on-ignition (LOI, %) was determined by ashing dried soils in muffle furnace at 550 °C for 4 hr (Nelson & Sommers, 1996). Organic carbon concentrations were measured on a Costech 4010 Elemental Analyzer.

2.3. Iron Sequential Extraction

The iron sequential extraction procedure was modified from previous studies (Amacher et al., 1990; Poulton & Canfield, 2005) to include removal of organic matter (Siregar et al., 2005). The extraction sequentially removed Fe loosely bound to particle surfaces (exchangeable; Amacher et al., 1990), Fe complexed by organic molecules (organic-bound; Siregar et al., 2005), short-range ordered Fe oxyhydroxides, crystalline Fe (oxyhydr)oxides, and magnetite Fe fractions (Poulton & Canfield, 2005). This extraction scheme was selected because hypochlorite minimally alters oxides (Siregar et al., 2005), hydroxylamine selective extracts short-range ordered phases (ferrihydrite and lepidocrocite), dithionite extracts the crystalline oxides remaining after SRO phases are extracted (hematite, goethite), and oxalate extracts the remaining magnetite. Note that when not used sequentially, citrate-buffered dithionite extracts ferrihydrite and lepidocrocite in addition to goethite and hematite, while oxalate extracts ferrihydrite and lepidocrocite in addition to magnetite (Poulton & Canfield, 2005).

Iron extractions were performed on ~1 g of wet soil. Exchangeable Fe was extracted with 10 ml of N_2-degassed barium chloride and ammonium chloride (0.1 M $BaCl_2$-NH_4Cl) in an anaerobic chamber for 20 min. The slurry was then centrifuged at 4,000 rcf for 30 min, and the supernatant was filtered (<0.45-μm nylon syringe filter) into 50-ml metal-free Falcon tubes. Organic-bound Fe was extracted twice for 6 hr each time with 10 ml of sodium hypochlorite (NaClO, 6% active Cl) acidified to pH 8 with hydrochloric acid. SRO Fe oxyhydroxides (ferrihydrite/lepidocrocite) were extracted with 10 ml of 1-M hydroxylamine-HCl in 25% *v*/v acetic acid for 48 hr. This extraction targets ferrihydrite and lepidocrocite but may also extract SRO goethite phases. Crystalline iron (oxyhydr)oxides (e.g., hematite and crystalline goethite) were extracted with freshly prepared citrate-buffered sodium dithionite solution (50-g/L sodium dithionite in 0.35-M acetic acid and 0.2-M sodium citrate buffer solution at pH 4.8) after mixing on the end-over-end shaker for 2 hr. The magnetite (Fe_3O_4) fraction was extracted with a 0.2-M ammonium oxalate and 0.17-M oxalic acid solution at pH 3.2 after 6 hr on the mechanical rotator. Between each step, soils were rinsed and

vortexed with 10-ml 0.01 M KCl solution, then centrifuged at 4,000 rcf for 30 min. Rinse solutions were filtered with a <0.45-μm syringe filter and combined with the filtered extract. Method blanks were collected and analyzed for each fraction. All extracts and matrix standards were stored at 4 °C until analyses.

2.4. Phosphorus Sequential Extraction

Phosphorus speciation was examined using a sequential extraction protocol developed for anoxic sediments that is complementary to the iron extraction protocol (Kinsman-Costello et al., 2014; Paludan & Jensen, 1995). Within each operationally defined fraction, phosphorus was differentiated as *molybdate reactive P*, which is approximately equivalent to inorganic phosphate (P_i), and *nonreactive P*, which is approximately equivalent to P contained in organic molecules (P_o). Reactive P was partitioned into water-soluble, dithionite-soluble (bound to reducible minerals such as Fe oxides and oxyhydroxides), and base-soluble (bound to nonreducible minerals such as Al oxides but containing some nonreactive inorganic P molecules such as pyrophosphates and polyphosphates; Reitzel et al., 2006) fractions. Average concentrations of dithionite-soluble Fe (= 14.6 ± 5.5 g/kg) far exceeded base-soluble Fe (= 0.76 ± 0.96 mg/kg), whereas base-soluble Al (= 1.2 ± 0.3 g/kg) was much higher than dithionite-soluble Al (= 0.19 ± 0.04 g/kg), supporting our interpretation of these mineral associations. Organic P was defined as the sum of water-soluble P_o, base-soluble P_o, and humic acids. Acid-soluble P represented P associated with Ca-bearing minerals, for example, apatite and calcium carbonates. Due to sample limitation, only water-soluble P was measured on APEX soils.

Phosphorus extractions were performed on ~1 g of wet soil. Water-soluble phosphorus was extracted with 25-ml deoxygenated ultrapure water (18 MΩ) in an anaerobic chamber for 1 hr. Soil-water slurries were centrifuged for 30 min at 4,000 rcf, and the supernatant was filtered through 0.45-μm syringe filters into clean centrifuge tubes. Iron-oxide-bound P was extracted with 25 ml of deoxygenated 0.11-M bicarbonate-buffered dithionite solution for 1 hr at 250 rpm. Filtered extracts were aerated for at least one hour, and then acidified with 1 M H_2SO_4. Base-soluble P was extracted with 25 ml of 0.1-M NaOH for 16 hr, and base extracts were acidified with 3 ml of 1 M H_2SO_4 to precipitate acid-insoluble organics, typically classified as humic acids. Acidified samples were filtered through glass fiber filters to remove the humic material, which was dried at 105 °C to determine mass, then ashed at 520 °C. Ashed material was digested with concentrated nitric acid in a hot block to solubilize P. Finally, acid-soluble P bound to apatite and other calcareous minerals was extracted with 25 ml of 0.5-M hydrochloric acid for 1 hr. Pellets were rinsed with 25 ml of deoxygenated ultrapure water between steps, and filtered rinses were combined with extracts and acidified with 1-M H_2SO_4. Reactive P was measured by the molybdenum blue method on a Lachat. Nonreactive P was determined as the difference between total P, measured by inductively coupled plasma optimal emission spectroscopy, and reactive P.

2.5. Phosphate Sorption Index

Phosphate sorption assays are used to quantify a soil's ability to sorb phosphate as a function of the concentration of dissolved phosphate in solution (Froelich, 1988). The phosphate sorption index (PSI) is a single-point adsorption value that provides a comparative measure of phosphate adsorption capacity across soils (Bache & Williams, 1971). Here ~4 g of wet soil from each soil horizon was mixed with 20 ml of N_2-degassed 75 mg/L P solution (as KH_2PO_4) and placed on a mechanical rotator in an anaerobic chamber for 24 hr. Each soil-solution suspension was filtered through a 0.45-μm polyethersulfone filter fitted with a 0.7-μm glass fiber prefilter. Dissolved phosphate was measured using the molybdate blue method by reacting a 100-factor diluted aliquot of the filtered solution with PhosVer 3 reagent (Hach) and measuring absorbance at 880 nm on a UV-Visible spectrophotometer (Shimadzu UV-1800). The residual soil was dried at 105 °C for 24 hr to determine dry soil mass (g). The amount of PO_4^{3-} sorbed to the soil (P_{sorbed}; mg/g) was calculated as the difference between the initial and final dissolved PO_4^{3-} mass in solution normalized to the dry soil mass. The PSI was calculated as 100 times the ratio of sorbed P (mg/g) to final log concentration of dissolved P in solution (μmol/L; (Bache & Williams, 1971).

2.6. X-Ray Absorption Spectroscopy

Iron K-edge X-ray absorption spectra were collected at 12-BM at the Advanced Photon Source (Argonne National Laboratory, Chicago, IL) in March 2018. Soils dried under N_2 atmosphere were transported to APS in sealed AnaeroPaks and transferred to an anaerobic chamber with Ar atmosphere. Soils were

packed into sample holders and sealed with Kapton tape. In addition to soils, we analyzed a series of reference compounds that were either purchased (iron (II) oxalate, iron (III) oxalate, iron (III) citrate), or synthesized following published protocols (ferrihydrite, goethite, and hematite; Schwertmann & Cornell, 2008). Powders were spread thinly onto Kapton tape.

The incident beam (~500 μm) was generated with a Si(111) monochromator to yield a reported flux of 4×10^{11} s^{-1} at 12 keV. Transmission and fluorescence spectra were collected concurrently using a N_2-filled FMB Oxford Ionization Chamber and a Canberra 13-element Ge detector, respectively. Spectra were collected from −150 to +547 eV around the Fe K-edge. All spectra were referenced to an Fe foil that was measured simultaneously in transmission mode.

Five individual spectra were collected from each soil sample on spots located 0.5 mm apart. Individual spectra were deglitched and merged to yield a single spectrum for each horizon. Three replicate scans were collected at a single position on all reference compounds. An energy shift of −0.9 eV was applied to all spectra to align the reference Fe foil (E0 = 7,111.65 eV) with the Fe standards database (E0 = 7,110.75 eV; Kraft et al., 1996). The E0 for each spectrum was set as the maximum of the first-derivative of μ(E). Linear combination fits were performed using Athena software following energy calibration, merging of replicate scans, background subtraction, and normalization (Ravel & Newville, 2005). Linear combination fits to normalized μ(E) spectra were performed from −20 to 30 eV around the Fe K-edge using single-valence standards to determine average Fe oxidation state. Linear combination fits to χ(k) spectra were performed from 3 to 12 A^{-1} with $R_{bkg} = 1$ to identify major Fe species. Standard spectra included the reference compounds listed above, plus iron (II) sulfide reported by the Advanced Light Source database.

2.7. Mössbauer Spectroscopy

Transmission ^{57}Fe Mössbauer spectroscopy was performed with a variable temperature He-cooled system with a 1,024-channel detector. A ^{57}Co source (~50 mCi or less) embedded in a Rh matrix was used at room temperature. Field-moist samples received at the University of Georgia frozen were defrosted inside a 5%/95% H_2/N_2 glove box. Once defrosted, samples were mounted (inside the glove box) between two pieces of 0.127-mm thickness Kapton tape and transferred immediately to the spectrometer cryostat for analysis at 5 K. Velocity (i.e., gamma ray energy) was calibrated using α-Fe foil at 295 K, and all center shifts (CSs) and peak positions are reported with respect to this standard. The transducer was operated in constant acceleration mode, and folding was performed to achieve a flat background.

Mössbauer spectral fitting of all spectra was performed using the Voigt-based fitting method (Rancourt & Ping, 1991) for quadrupole splitting distributions and combined hyperfine field distributions, as implemented in the Recoil™ software, ISA Inc. All Voigt-based fitting Mössbauer parameter definitions and a description of the relevant notation are given by Rancourt and Ping (1991). Mössbauer fitting parameter errors are two-standard deviation (2σ), as calculated by Recoil™. In reporting quantitative phase abundances or site populations it is assumed that the Mössbauer recoilless fractions of all detected phases or Fe-bearing components are equal, such that subspectral areas (expressed as fractions of total spectral area) are equal to the amounts of Fe (expressed as fractions of total Fe) in the corresponding phases or components. This assumption is expected to be valid at cryogenic temperatures (Lalonde et al., 1998; Rancourt, 1998). More detailed information regarding spectral assignments is provided in the supporting information.

2.8. Data Analysis and Statistics

Extract solutions were analyzed by inductively coupled plasma optical emission spectrophotometry (PerkinElmer 8000, ICP-OES). Calibration standards were prepared separately for each fraction in solutions matching the matrix of the extract solutions. Method blanks were analyzed to ensure negligible contamination from extraction chemicals and the extraction process. Values equal to half the lowest calibration standard were used to represent concentrations that were below the detection limit in calculations. Element concentrations in extract solutions were converted to soil concentrations (on a dry weight basis). Because extraction procedures were performed using wet samples, gravimetric water content (g H_2O g-dry $soil^{-1}$) was used to convert wet soil mass to dry soil mass.

All statistical analyses were performed in R. Variables were transformed as necessary to better meet the assumptions for linear models. Iron concentrations were log-transformed, while proportions of Fe and P

were logit-transformed. Pearson product-moment correlation tests were used to determine significant correlations between measured variables. To assess which soils characteristics best predicted PSI, we conducted a model selection procedure using candidate models that included both the values and relative proportions of Fe species, Al species, and soil pH, VWC, and %C as predictors. We developed candidate models using the leaps (v3.0) package in R statistical software, which identifies the best models out of an exhaustive search of all possible combinations of predictors. We specified leaps to return the four best models with one term, two terms, three terms, and four terms, out of the entire list of predictor variables. After testing each model for multicollinearity and omitting terms with variance inflation factors greater than 2, we used Akaike's Information Criterion (AIC) to generate weights to identify the best supported models out of the candidate list (more details in supporting information).

3. Results

3.1. Soil Characteristics

To explore hydrologic controls on Fe-P interactions, we examined the geochemical composition of surface organic soils collected from plots with contrasting soil saturation within four long-term experimental sites that span tundra and boreal ecosystems (Figure 1). Soils across all plots were organic rich (39 ± 9 wt.% organic C) and ranged from highly acidic (pH ~ 3) to circumneutral (~6.4; Table 1). In general, soils occupying topographic high points were acidic and dry relative to soils occupying topographic lows, and hillslope-scale topography (e.g., MEF bog versus fen and TFS tussock/heath versus wet sedge) drove larger pH gradients than microtopography (e.g., BEO polygon features and MEF hummock versus hollow). At the APEX site, where saturation gradients were induced by water table manipulation rather than topography, soil characteristics were similar across all plots. Soil pH values measured for TFS sites (ranged 5.0 for heath and tussock tundra to 6.2 for wet sedge) were slightly higher than previously reported values (3.7–5 for heath and tussock tundra to 5.8 for wet sedge) but still lower than soil pH reported for comparable but younger nonacidic sites (pH 6–6.5 for tussock tundra; Shaver et al., 2014; Whittinghill & Hobbie, 2011). For all data reported in this manuscript, uncertainties represent standard error of the mean for each plot or standard deviation for values averaged across multiple plots.

3.2. Iron Speciation in Tundra and Boreal Peat Soils

Our first objective was to quantify soil Fe reservoirs and evaluate controls on Fe speciation using sequential extractions and spectroscopy. On average, iron (oxyhydr)oxides, consisting of both SRO (hydroxylamine-extractable; 27 ± 21%) and crystalline (dithionite-extractable; 23 ± 29%) (oxyhydr)oxides, comprised one half of extractable Fe (Figure 2 and Table S1). Organic-bound Fe (hypochlorite-extractable) accounted for most of the remainder (42 ± 29%), while another 7 ± 12% consisted of exchangeable Fe. Oxalate-extractable Fe was a minor component (1.5 ± 2.2%).

Total extractable Fe increased with increasing pH across all sites ($r = 0.62$, $p < 0.0001$). The high pH wet sedge (mean 6.2 ± 0.1) had at least an order of magnitude higher Fe concentrations (166 ± 14 g Fe kg-soil^{-1}) than all other plots, including both the more acidic heath (14.2 ± 7.4 g Fe kg-soil^{-1}) and tussock tundra (2.56 ± 5.28 g Fe kg-soil^{-1}) plots within TFS. Similarly, circumneutral fens were Fe-rich (mean pH 6.3 ± 0.2; 13.6 ± 4.1 g Fe kg-soil^{-1}) relative to acidic bogs (mean pH 3.0 ± 0.1; 1.08 ± 0.17 g Fe kg-soil^{-1}) at MEF. Extractable Fe was less variable at APEX and BEO, which exhibited small to negligible pH gradients amongst plots.

Soil pH also largely explained how Fe was partitioned between different fractions. Iron (oxyhydr)oxides increased with increasing pH ($r = 0.61$, $p < 0.0001$). This trend was driven by increases in both the absolute value and proportion of SRO Fe oxyhydroxides at higher pH ($r = 0.64$ and $r = 0.52$, respectively, $p < 0.0001$), while the proportion of crystalline Fe (oxyhydr)oxides was not pH-dependent. Iron (oxyhydr)oxides comprised the majority of extracted Fe in the bog hummocks and fen (MEF) and in the heath and wet sedge soils (TFS). Of these, SRO Fe was relatively high in the circumneutral, Fe-rich fen (43 ± 10%) and wet sedge (68 ± 1%) while crystalline Fe dominated the more acidic, Fe-poor bog hummock (91 ± 2%) and heath soils (69 ± 6%). Iron (oxyhydr)oxides consisted primarily of SRO phases (<5% crystalline Fe) at BEO and APEX, but these were as or less abundant than organic-bound Fe. Although the APEX fen receives groundwater discharge (Racine & Walters, 1994), its acidic soils favored organic complexes over oxyhydroxides.

Table 1
Properties (± s.e.m.) of Surface Soils Collected From Different Landscape Features at Four Arctic and Boreal Sites

		Soil pH		VWC (g H_2O cm^{-3})		Loss on ignition (wt.%)		Carbon (wt.%)		Phosphate sorption index	
Site	Plot	**Average**	±	**Average**	±	**Average**	±	**Average**	±	**Average**	±
Barrow Environmental Observatory (BEO)	Low-center polygon, Center	4.36	0.12	0.36	0.13	48.3	19.3	26.0	9.4	51	5
	Low-center polygon, Ridge	4.06	0.01	0.12	0.01	89.6	2.3	42.5	0.5	80	9
	Low-center polygon, Trough	4.9	0.1	0.57	0.17	56.7	17.2	29.7	7.7	86	18
	High-center polygon, Center	3.93	0.07	0.12	0.02	75.5	6.5	28.4	11.3	34	4
	High-center polygon, Trough	4.98	0.08	0.42	0.02	64.9	6.5	32.7	2.7	63	7
Toolik Field Station (TFS)	Tussock Tundra	5.4	0.05	0.07	0.01	89.0	0.7	45.0	1.1	11	1
	Hilltop heath	4.99	0.24	0.15	0.05	44.4	11.5	22.4	5.6	14	2
	Wet Sedge	6.16	0.07	0.81	0.06	57.9	0.8	28.4	0.8	158	11
Alaska Peatland Experiment (APEX)	Lowered water table	4.58	0.06	0.24	0.01	84.2	0.9	40.1	0.6	50	1
	Raised water table	4.82	0.05	0.20	0.04	87.9	1.5	43.1	0.9	54	4
	Control site	4.44	0.02	0.22	0.02	82.0	0.8	41.1	0.5	40	<1
Marcell Experimental Forest (MEF)	Site 1: Bog hummock	2.96	0	0.15	n.a.	97.6	0.0	46.9	n.a.	0.2	1.5
	Site 1: Bog hollow	3.05	0.01	0.31	0.02	91.7	2.5	45.5	0.2	16	2
	Site 2: Bog hummock	3.01	0.12	0.12	0.02	96.6	0.2	47.8	0.4	3.8	1.0
	Site 2: Bog hollow	2.9	0.01	0.12	0.02	92.4	0.4	47.1	0.8	15	2
	Site 3: Fen hummock	6.4	0.11	0.30	0.06	81.0	2.7	41.7	0.8	59	15
	Site 3: Fen hollow	6.19	0.02	0.23	0.01	86.4	1.4	43.4	0.9	40	8

Note. Volumetric water content was calculated as gravimetric water content × bulk density, where bulk density was determined following the equation from Bockheim et al. (2003) as follows: SOC (%) = −9.7872*ln (bulk density, g/cm^3) + 8.2432.

Correspondingly, the proportion of organic-bound Fe generally decreased with increasing pH. These results are consistent with previous observations that organic soils contain increasing amounts of Fe (oxyhydr)oxides relative to Fe (III)-organic complexes with increasing pH (Karlsson et al., 2008; Karlsson & Persson, 2010; Sundman et al., 2014). As such, organic-bound Fe was the most abundant fraction in the acidic MEF bog hollows (68 ± 4%), APEX peat (79 ± 3%), TFS tussock tundra (48 ± 3), BEO low-centered polygon ridge (67 ± 10%), and high-centered polygon center (75 ± 17%) plots. Iron-poor bog hummocks, which were highly acidic but dominated by crystalline Fe (91 ± 2%) rather than organic-bound Fe, were the only exception to this trend. When bog hummock soils were omitted from the analysis, the proportion of organic-bound Fe was significantly negatively correlated to pH ($r = -0.58$, $p < 0.0001$).

X-ray absorption and Mössbauer spectroscopies were used to identify Fe species and support interpretation of operationally defined extractions. All soils contained mostly Fe (III) (83 ± 12%), as determined by LCF fits to the XANES region (Table S2). First-derivative maxima (~7,123–7,126 eV) were consistent with organic-bound Fe^{3+} and Fe (III) oxyhydroxides, with secondary peaks at ~7,119 eV indicative of lesser Fe (II) contributions (Figure 3; O'Day et al., 2004). EXAFS spectra were best fit by a combination of ferrihydrite, goethite, and Fe^{3+}-citrate standards (Table S3). The relative proportion of organic-bound Fe to Fe (oxyhydr)oxides was determined by the ratio of the Fe-O to Fe-Fe scattering peaks (Figure 3). Higher ratios, reflecting smaller Fe-Fe scattering peaks, indicated higher proportions of organic-bound Fe (Figure S1 and Table S3). Soils dominated by extractable Fe (oxyhydr)oxides had more intense Fe-Fe scattering peaks and lower Fe-O to Fe-Fe ratios than soils dominated by organic-bound and/or exchangeable Fe. These results provide additional evidence that soils contained a mix of organic-bound Fe (III) and Fe (III) (oxyhydr)oxides that varied across landscape positions.

MBS spectra obtained for the MEF soils supported these interpretations. Fen soils exhibited sextets indicative of high proportions of oxyhydroxides (ferrihydrite with lesser nanogoethite), while acidic bog hollows were dominated by prominent doublets likely representing organic-bound Fe^{II} and Fe^{III} (Figure 4 and Tables S4–S7). For example, the S2 bog hollow soil contained ~65% ferrous Fe and this component had MBS parameters (CS ~ 1.4 and QS ~ 3.3 at 5 K) that strongly suggest a high degree of organic complexation, although we cannot exclude potential contributions from Fe-substituted in clay minerals (Chen & Thompson, 2018). The fens contained lesser amounts of organically complexed (or clay mineral) Fe^{II} and Fe^{III} (<11%) but high proportions of SRO oxyhydroxides and a highly disordered phase ((b)OxHy) that

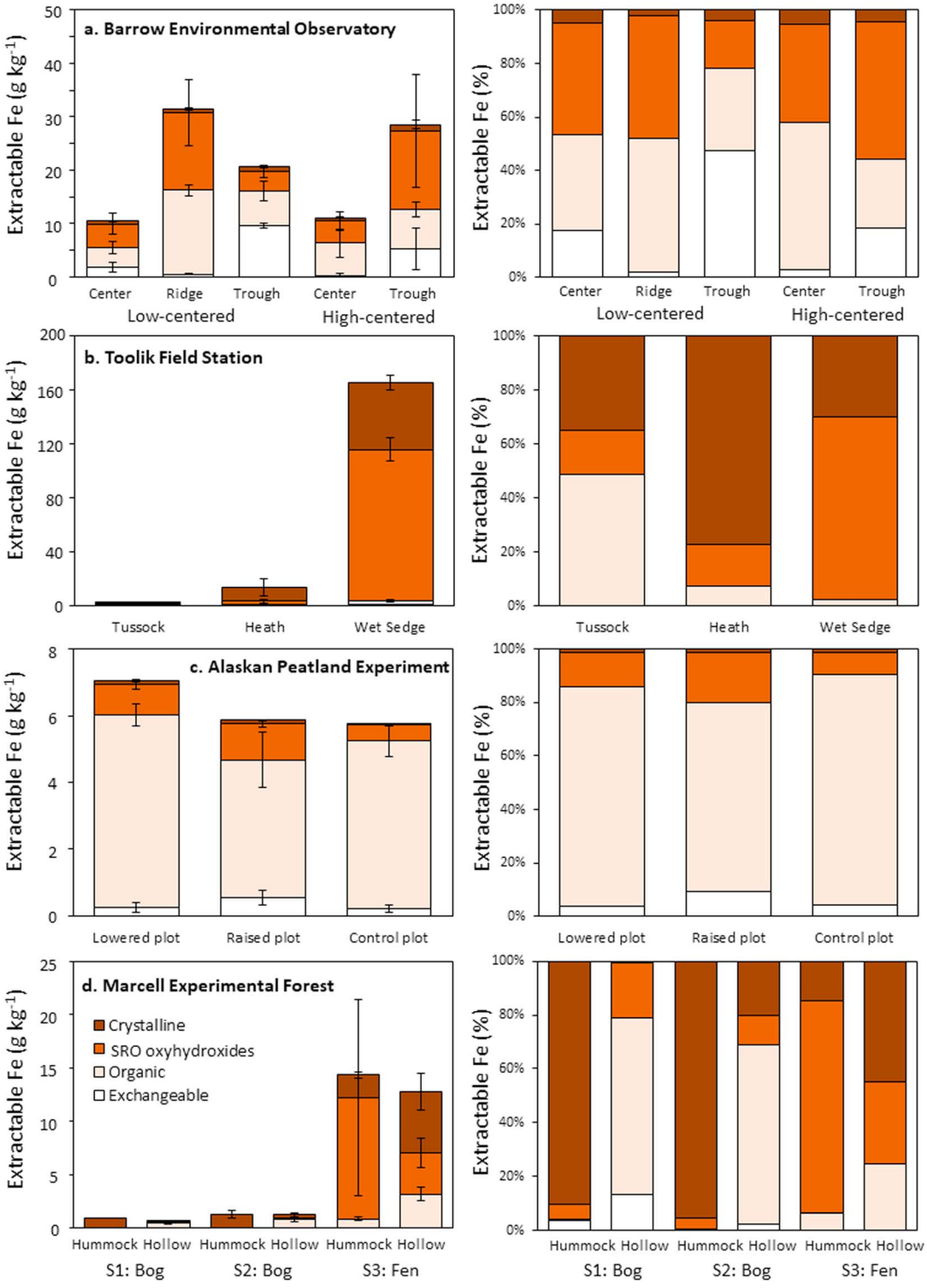

Figure 2. (left panels) Concentrations (mean ± s.e.m.) and (right panels) proportions of Fe extracted in exchangeable, organic-bound, short-range ordered oxyhydroxide, and crystalline (oxyhydr)oxide fractions from surface soils of characteristic topographic features at each site. Oxalate-extractable (magnetite + potential silicate dissolution) Fe represented <5% of extracted Fe and is not shown. The legend shown in panel (d) applies to all panels. Each bar represents the average of soils collected in triplicate from indicated landscape features. The *y* axes of the four left panels differ in scales to illustrate patterns within geographic sites.

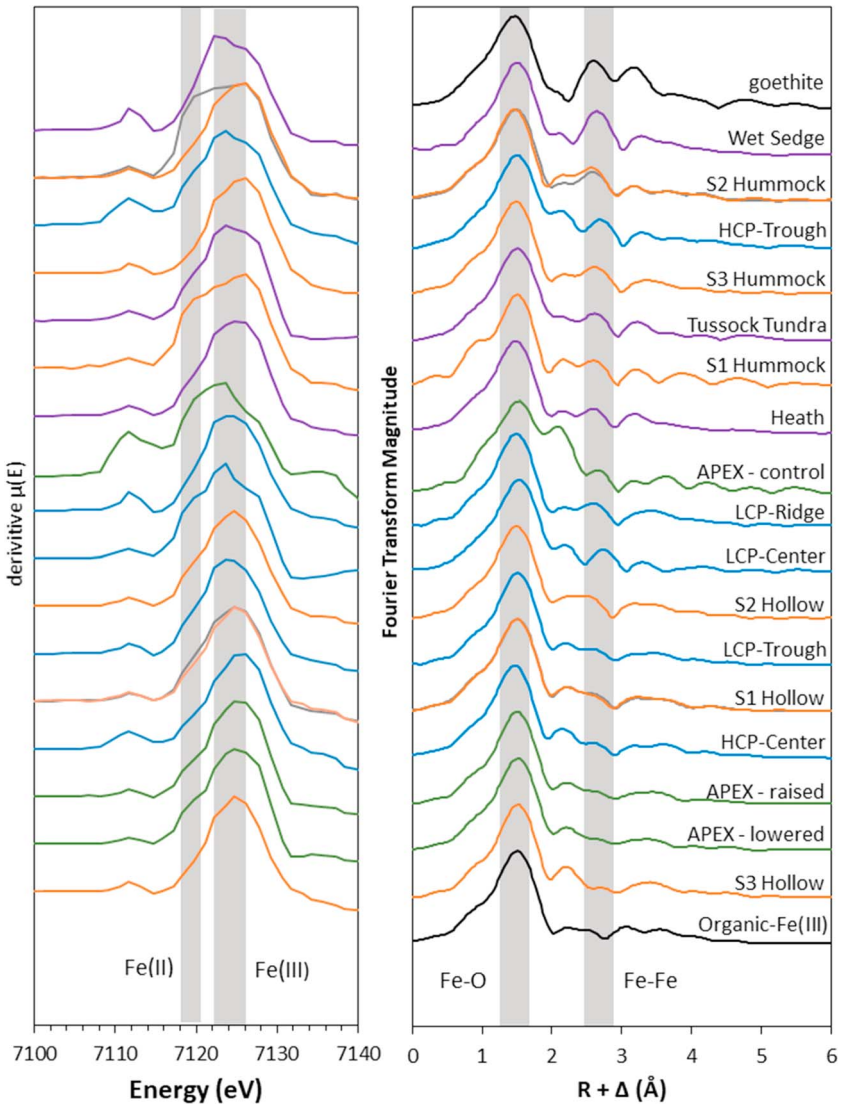

Figure 3. Iron K-edge X-ray absorption spectra plotted as (left panel) the XANES derivative and (right panel) the Fourier-transformed EXAFS. Spectra are color coded by site: blue (BEO), purple (TFS), green (APEX), and orange (MEF). Vertical gray bars indicate positions of (left panel) Fe^{II} and Fe^{III} derivative maxima or the (right panel) Fe-O (~1.5 Å) and Fe-Fe (~2.7 Å) scattering peaks. Sample spectra are arranged from top to bottom by the ratio of the Fe-O peak intensity to the Fe-Fe peak intensity, such that the standard goethite spectrum is at the top (high Fe-Fe scattering peak and low ratio) and organic-Fe (III) is at the bottom (high ratio). Spectra obtained for replicate soils of the S2 bog hummock and S1 bog hollow are shown as gray overlay.

may correspond to amorphous iron (hydr)oxides coprecipitated with organic matter. An oxide component consistent with hematite dominated the weak Fe signal in the S2 bog hummock and may indicate inputs of mineral dust from local uplands. Detailed information regarding assignment of spectral components is provided in the supporting information.

In the fen hollow, high proportions of Fe oxyhydroxides measured by sequential extractions and MBS coupled with high proportions of organic-bound Fe measured by XAS may indicate an abundance of organically complexed, nanoparticulate Fe (oxyhydr)oxides. The MEF fen hollow had the lowest Fe-Fe scattering peak in EXAFS (Figure 3) despite high proportions of oxide-extracted Fe (Figure 2) and a prominent oxyhydroxide (ferrihydrite and goethite) sextet in Mössbauer (Figure 4). This result may be explained by the different scales probed by each technique. XAS records the average coordination environment surrounding all Fe atoms (Newville, 2014). For nanoparticles with a high surface area to volume ratio, a substantial

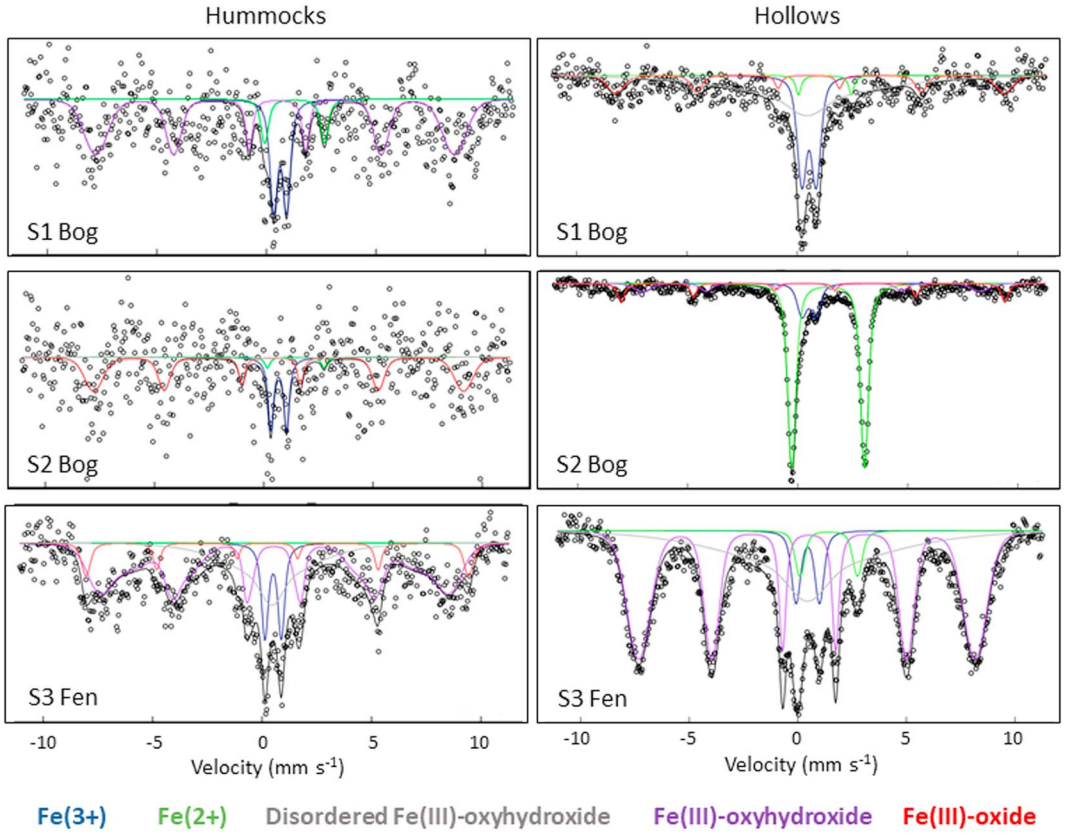

Figure 4. Mössbauer spectra obtained from individual replicates of MEF soils. Symbols represent data collection, and lines represent best fits of different components indicated in the legend. Population abundances (Table S4 with additional details reported in Tables S5–S7) are reported with higher certainty for the hollows and S3 fen hummock than for the S1 and S2 hummocks.

proportion of Fe atoms will be in close proximity to C atoms at the mineral surface and appear to be organic bound. In comparison, Mössbauer records the crystalline order of each mineral regardless of bonding environment and is sensitive to the crystallinity of nanoparticles. Together, these results indicate that that organically complexed, nanoparticulate Fe (oxyhydr)oxides may be especially prevalent in these fen soils. The contribution of nanoparticulate Fe to organic-associated Fe in the other sites remains unknown and warrants further investigation.

3.3. Phosphate Sorption Capacity

Phosphate sorption capacity, as compared across soils using a PSI, was strongly related to SRO Fe oxyhydroxides. PSI values were best explained by statistical models that included positive correlations with SRO Fe oxyhydroxides (or total extractable Fe) and exchangeable Fe but a negative correlation with aluminum (Al) in SRO phases (Table S8). Specifically, PSI increased linearly with log-scale increases in SRO Fe ($R^2 = 0.59$; $p < 0.0001$; Figure 5a). Wet sedge soils from TFS possessed both exceptionally high concentrations of SRO Fe oxyhydroxides (112 ± 8 g Fe kg-soil^{-1}) and the highest sorption capacity of any site (PSI = 158 ± 11 stdev). In contrast, MEF bog soils and TFS upland soils (tussock tundra and heath) had low concentrations of SRO Fe oxyhydroxides (average = 0.62 ± 0.26 g Fe kg-soil^{-1}) and exhibited the lowest sorption capacities (PSI ≤ 20). The negative relationship between PSI and the proportion of Al in SRO phases conflicts with numerous instances in the literature demonstrating positive relationships between indicators of SRO Al oxides (usually oxalate-extractable Al) and PSI (e.g., Darke and Walbridge (2000)) and underscores the importance of Fe (oxyhydr)oxides relative to Al (hydr)oxides to phosphate sorption in these organic-rich systems.

PSI generally decreased as iron oxide crystallinity increased, indicating that (oxyhydr)oxide crystallinity was an important factor controlling phosphate sorption capacity (Strauss et al., 1997). Specifically, there was a

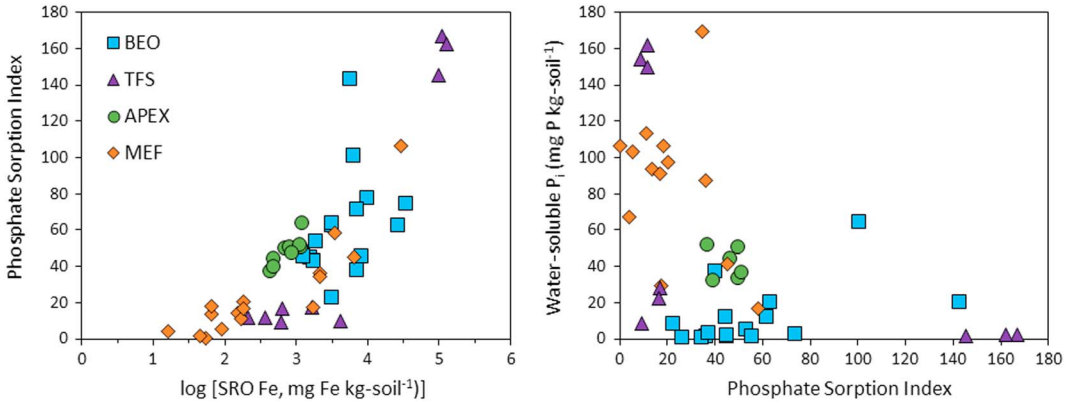

Figure 5. (left) Phosphate sorption index, a parameter comparing the sorptive capacity of different soils for phosphate, increased with increasing log concentrations of Fe contained in short-range ordered iron oxyhydroxides ($r = 0.78$; $p < 0.0001$) extracted with hydroxylamine hydrochloride. (right) Water-soluble phosphate, the most bioavailable form of phosphorus, decreased with increasing PSI ($r = -0.51$; $p < 0.001$).

significant positive correlation between PSI and the percent of Fe in SRO Fe oxyhydroxides ($r = 0.60$, $p < 0.0001$), and a trend toward a negative correlation with the percent of Fe in crystalline Fe oxides ($r = -0.23$, $p = 0.07$). As one example, MEF bog hollows had more SRO Fe (both g/kg and %) and higher PSI than bog hummocks. Bog hummocks had relatively high concentrations of crystalline Fe but lower PSI.

Soil pH was also positively correlated with PSI ($p < 0.001$, $r = 0.48$; Figure S2) but explained only 23% of the variation. It is likely that pH influenced PSI by controlling Fe oxyhydroxide precipitation and may also covary with factors determining Fe abundance, for example, as an indicator of groundwater inputs. Subsequently, phosphate sorption capacity was directly shaped by the quantity and form(s) of Fe present. Although phosphate sorption was generally expected to increase with decreasing pH (Strauss et al., 1997), this effect was secondary to higher concentrations of SRO Fe oxyhydroxides at circumneutral pH in these soils.

Organic-bound Fe (hypochlorite-extractable) was not included in either of the best models predicting PSI across sites but was the second best predictor of PSI in the BEO soils (AIC weight = 0.33) after total extractable Fe (AIC weight = 0.37). Despite the fact that BEO organic soils contained relevant fractions of SRO Fe (ranged from 14% to 62% of extracted Fe), a linear model predicting PSI from SRO Fe was not statistically significant when these plots were examined in isolation ($p > 0.05$). Although considerable unexplained variance remained in these models ($R^2 = 0.28$, $p = 0.04$), model predictions improve for total extractable Fe ($R^2 = 0.41$) and organic Fe ($R^2 = 0.50$) when a single outlier (one LCP trough replicate with very high PSI) was omitted.

3.4. Phosphorus Speciation in Organic Surface Soils

On average across all organic soils, 28% ± 13% of extractable P and 46% ± 2% of extracted inorganic P (P_i) was bound to iron (oxyhydr)oxides (dithionite-extractable; Figure 6 and Table S9). This P_i represents a substantial pool of phosphate that has the potential to be released during reductive dissolution of iron oxyhydroxides in anoxic conditions. Another 16% ± 14% of P_i was water soluble (8% ± 8% of total P), while 30% ± 22% was bound to nonreducible aluminum (hydr)oxides (base soluble; 19% ± 17% of total P). Phosphate bound to nonreducible aluminum (hydr)oxides could represent stable mineral-bound P that is not sensitive to redox fluctuations. Phosphorus contained in organic molecules comprised 37% ± 18% of extracted P, with P associated with Ca-bearing minerals (acid soluble) constituting the remaining 7% ± 15%. Acid-soluble P was highly variable across BEO soils (18% ± 25% of extracted P) and highest in the mineral-rich HCP center soil but uniformly low in TFS and MEF soils (1.4% ± 1.4% of extracted P).

Water-soluble P_i, the most bioavailable of the P fractions, decreased with increasing soil PSI ($r = -0.51$, $p < 0.001$, Figure 5b). That is, soils with a high capacity to bind phosphate had both low concentrations of water-soluble P_i and a low percentage of P_i in the water-soluble fraction. This trend is particularly evident

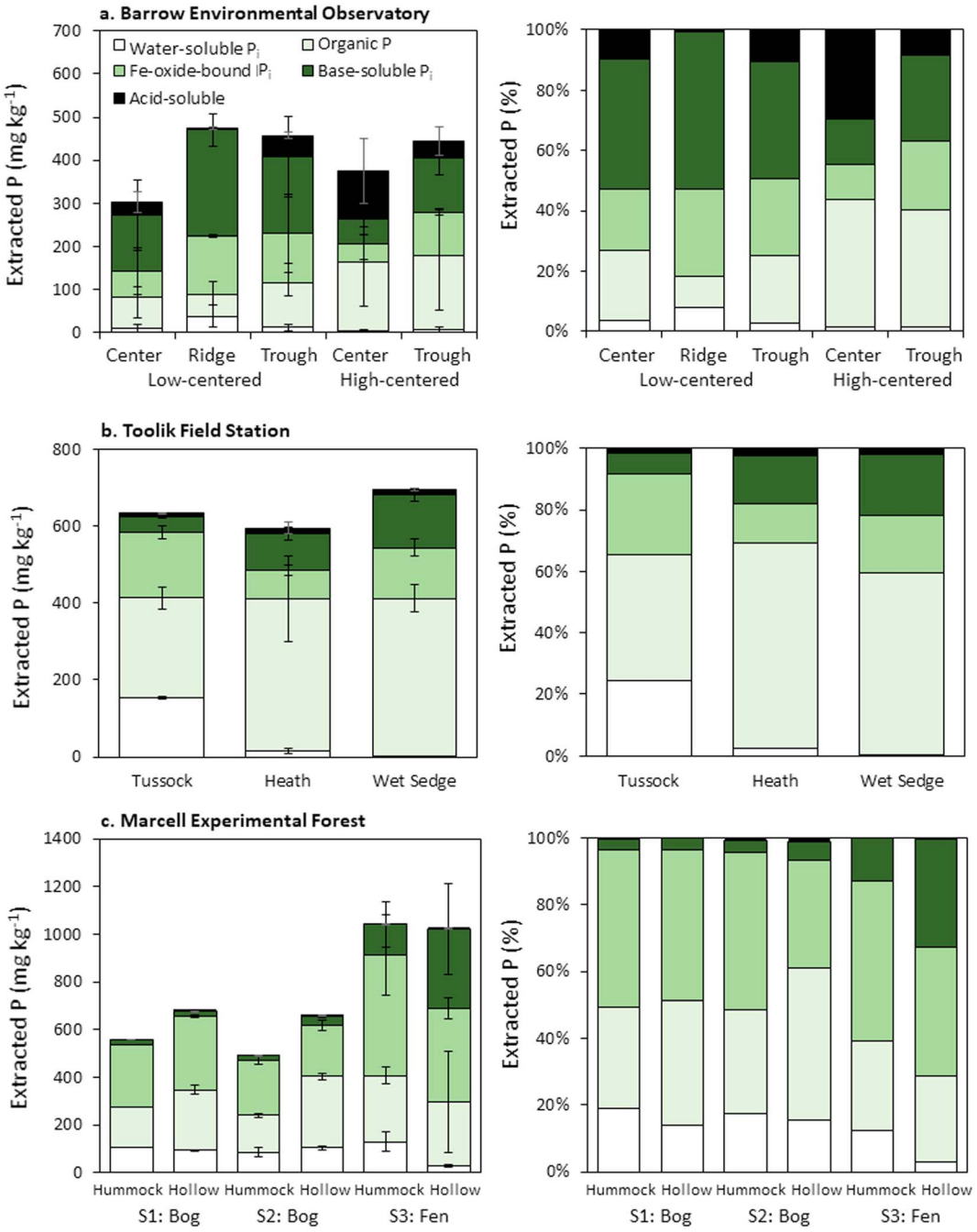

Figure 6. (left panel) Concentrations and (right panel) proportions of extracted soil phosphorus. Extracted P was dominated by organic P (P_o) and oxide-bound phosphate (Fe-oxide-bound P_i and base-soluble P_i) with smaller amounts of water-soluble and acid-soluble P_i. Organic P includes nonreactive phosphorus from water-soluble, base-soluble, and humic acid fractions. Each bar represents the average (± standard error of the mean) concentration measured in soils collected in triplicate from each landscape feature.

across the TFS hillslope, where upland tussock tundra had low PSI and high water-soluble P_i (155 ± 3 mg P kg-soil^{-1}, 25% ± 2%), while low-lying wet sedge soils had high PSI and negligible water-soluble P_i. Similarly, the low-PSI bog soils had higher water-soluble P_i (97 ± 5 mg P kg-soil^{-1}, 16% ± 1% of extracted P) than the high-PSI fen soils (69 ± 28 mg P kg-soil^{-1}, 7% ± 2%) at MEF. Water-soluble P_i was uniformly low across BEO soils (<12 mg P kg-soil^{-1}; <5% of extracted P), with the exception of the low-centered polygon ridge

(= 38 ± 26 mg P kg-soil^{-1}; 12% of extracted P). These trends are evident despite the expectation that water-soluble P_i varies over the growing season.

BEO soils had higher average concentrations (147 ± 30 mg P kg-soil^{-1}) and proportions (25% ± 4%) of base-soluble P_i than the other sites, suggesting that more of the P was sequestered in tightly bound, nonredox sensitive mineral forms (e.g., Al oxides) that may be unavailable to organisms over long-time scales. The high proportions of base-soluble P_i in the Barrow soils were likely due to their high mineral content, given that even the organic horizons contain primary minerals or are in close contact with mineral soil (Herndon et al., 2017). Similar proximity to mineral soil may explain base-soluble P trends at other sites. For example, base-soluble P_i increased from the tussock tundra (6% ± 1%) to the heath and wet sedge plots (18% ± 2%) at TFS. At MEF, base-soluble P_i was uniformly low across the bogs (<6%) but variable (4%–53%) in the fen.

A high mineral content can also explain the relatively large quantities of acid-soluble P (Ca-associated) in BEO soils (Figure 6). Acid-soluble P represents phosphate in calcareous minerals that is released into solution during mineral weathering. In contrast to base-soluble P_i, acid-soluble P is generally considered to be more accessible to organisms (Vitousek et al., 2010; Walker & Syers, 1976) and may serve as a P source in BEO soils.

4. Discussion

In this study, we evaluated environmental controls on Fe speciation in organic soils, and in turn, how Fe speciation regulated both actual and potential phosphate sorption. Across all sites, topography drove broad patterns of Fe leaching and accumulation in soils by modulating redox and pH gradients. Iron (oxyhydr)oxides were most abundant in circumneutral saturated depressions (Figure 2), likely due to accumulation at near-surface redox interfaces. We infer that dissolved Fe^{2+} flowed into topographic lows from upland leaching and/or groundwater inputs and migrated through anoxic zones toward the soil surface where it oxidized to Fe^{3+} and either precipitated as Fe^{III} oxyhydroxides or was complexed by organic matter (Figure 7). Low-lying soils had more circumneutral pH due to inputs of alkalinity from groundwater or mineral weathering, facilitating accumulation of iron oxyhydroxides relative to organic-bound Fe. Upland soils were more acidic and better drained, facilitating Fe leaching and/or complexation by organic matter.

This conceptual model for landscape-scale Fe accumulation and speciation may be influenced by factors other than topography that modify soil pH and hydrology across more varied tundra and boreal ecosystems. For example, in the Toolik region, soil pH tracks with land surface age, which is determined by time since glaciation. Tussock tundra soils are circumneutral (~6.5) and calcium-rich in recently glaciated areas but acidic (<5.5) and base-cation depleted on older land surfaces that have experienced more weathering (Whittinghill & Hobbie, 2011). Older soils are also relatively enriched in Fe and Al minerals that adsorb organic molecules and can store up to 55% of soil C (Hobara et al., 2016). Topographic controls on soil pH, and consequently Fe leaching and accumulation patterns, may therefore differ in different regions due to contrasts in underlying lithology and weathering extent. Although more research is needed to evaluate these differences, it is expected that younger, nonacidic soils would exhibit less Fe transformation and hillslope transport.

The formation and dissolution of Fe oxyhydroxides may be a particularly important control on P cycling in these systems. These minerals provide abundant surface area to which phosphate can bind and become at least temporarily unavailable to plants and microorganisms. Indeed, soluble phosphate was low in Fe-oxyhydroxide-rich soils that had high capacities to bind phosphate (Figure 5). This result is consistent with previous studies from the Toolik Field Station demonstrating that P-limitation is more common in wet sedge tundra than in other tundra systems (Nadelhoffer et al., 1991; Shaver & Chapin, 1995). Thus, we contend that geochemical sorption can effectively *compete* with biological uptake for available phosphate, even in organic soils. Low-lying soils that accumulate iron oxyhydroxides may form nutrient traps and serve as barriers to phosphate transport into adjacent streams and lakes (Zak et al., 2004). Although previous studies have suggested that organically complexed Fe^{3+} can effectively bind phosphate (Kizewski et al., 2010), organic-bound Fe was significantly correlated with PSI only in BEO soils. It is possible that the specific nature of organic-bound Fe in the BEO soils enhances phosphate sorption capacity in a manner not present at the other sites, but the mechanism cannot be determined by this study.

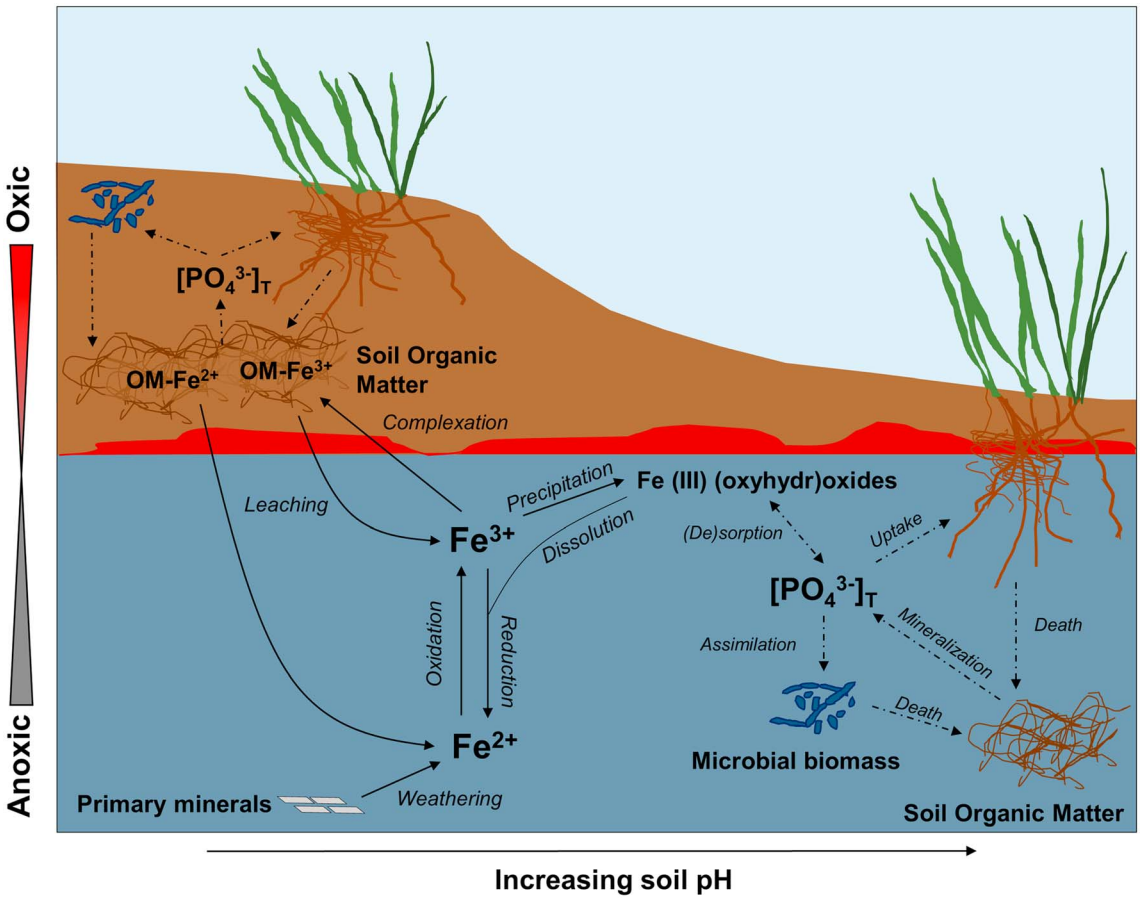

Figure 7. Conceptual diagram of coupled interactions between iron and phosphorus across topographic and saturation gradients in peatlands. Iron, present largely as organic-complexes in acidic soils, is leached from topographic highs and transported as dissolved Fe to more circumneutral topographic lows where Fe oxyhydroxides precipitate at redox interfaces. These Fe oxyhydroxides compete with plants and microorganisms for phosphate that is enzymatically cleaved from soil organic matter (*mineralization*). Solid and dashed arrows indicate transport and transformation processes for Fe and P, respectively. Generalized redox and pH gradients are indicated. Dissolved phosphate species ($[PO_4^{3-}]_T$) include all pH dependent variations. Permafrost, which inhibits drainage in many of these ecosystems, is not shown.

Relatively acidic soils that were dominated by organic-bound or crystalline Fe phases had high concentrations of soluble phosphate and low phosphate sorption capacities. Although phosphate solubility can vary seasonally (Weintraub & Schimel, 2005), this trend provides evidence that upland and/or acidic soils may contain more bioavailable P because they lack sufficient iron minerals to compete with biological uptake. Indeed, heath and tussock tundra are generally reported to be N or N + P limited rather than P limited (Nadelhoffer et al., 1991; Shaver & Chapin, 1995). We hypothesize that plant and microbial uptake rather than geochemical processes regulate P solubility in these soils. However, although crystalline Fe oxides have lower sorption capacity than SRO Fe oxyhydroxides, they are more resistant to reductive dissolution (Chen et al., 2018) and may sequester bound phosphate for longer timescales. The propensity for crystalline Fe oxides to resist dissolution has been implicated in its potential to stabilize SOM for longer time periods than the relatively transient stabilization provided by SRO Fe oxides (Hall et al., 2018).

Although half of soil phosphate was associated with iron (oxyhydr)oxides (Figure 6), the amount of Fe-bound P_i was not related to the amount of iron (oxyhydr)oxides in a given soil. There are a few possible explanations for these results. First, dithionite extracts both SRO and crystalline Fe (oxyhydr)oxides (Poulton & Canfield, 2005); therefore, P derived from crystalline oxides, which have lower sorption capacity (Wang et al., 2013), may obscure correlations between PSI and P bound to SRO Fe oxyhydroxides. There may also be factors other than mineral abundance that control phosphate sorption. For example, although soils may be enriched in SRO Fe phases that confer a high capacity to bind phosphate, there may only be a small

amount of phosphate able to bind at any given time. The capacity for soil to bind phosphate likely exceeds the amount of phosphate present in these low-nutrient soils. Third, Fe (oxyhydr)oxides that experience fluctuating redox conditions may provide only a temporary sink for phosphate. Reductive dissolution of iron oxyhydroxides during periods of anoxia may release phosphate into solution and prevent long-term accumulation. Short-range ordered Fe phases that preferentially accumulate in poorly drained soils are prone to rapid dissolution, consequently mobilizing aqueous phosphate and Fe-cemented P-bearing colloids (Bridgham et al., 1998; Chen et al., 2018; Henderson et al., 2012).

We infer that the capacity for Fe-rich soils to bind phosphate currently exceeds the amount of phosphate that is available to bind in these nutrient-limited ecosystems. That is, Fe oxyhydroxides effectively bind soluble phosphate, but other ecosystem processes restrict phosphate release into solution. However, soils enriched in Fe oxyhydroxides have a marked potential to serve as future sinks for phosphate as decomposition of organic matter accelerates and releases increasing amounts of P (Chapin et al., 1995). Widespread soil drainage and oxidation may facilitate iron oxyhydroxide precipitation and further increase phosphate sorption capacity. Given that Fe-rich soils often occupy low-lying positions on the landscape, Fe minerals may serve as nutrient traps that limit local bioavailability and transport to downstream water bodies.

The turnover time of Fe-bound phosphate, which is largely unavailable for biological cycling, remains unclear. Phosphate can readily sorb to SRO Fe oxyhydroxides that precipitate during wetland drainage or be released into solution as iron (oxyhydr)oxides dissolve during transient anoxic conditions (Henderson et al., 2012; Kinsman-Costello et al., 2014; Zak et al., 2004). In this capacity, these minerals can serve as both sinks and sources of bioavailable phosphate as water tables fluctuate. For example, rapid immobilization of phosphate solubilized during anoxic incubation of tropical soils was attributed to microbial uptake (Lin et al., 2018). Additional laboratory and field experiments should explore biological acquisition of oxide-bound phosphate and transfer between biotic and abiotic pools. It is possible that instead of limiting bioavailability, Fe minerals may provide important phosphate reservoirs in these P-limited systems. Interactions between Fe and P are important to study given that nutrient availability may dictate whether terrestrial ecosystems act as sinks or sources of C (Wieder et al., 2015). Increased decomposition rates under warming climate may contribute to formation of Fe-P associations by releasing organic-complexed Fe that can precipitate to form oxyhydroxide minerals and by accelerating release of phosphate into solution that can bind to Fe oxyhydroxides before biological assimilation. These processes may be exacerbated as increased rates of evapotranspiration and lowering water tables produce drier and more oxidized surface soils that favor decomposition and Fe oxidation.

Acknowledgments
The authors thank Anne Giblin for samples collected from near the Toolik Field Station, Bree Richardson for help with soluble reactive phosphorus analysis, and Maximilian Barczok and Chelsea Smith for assistance with soil carbon, sequential extraction, and X-ray absorption data collection. This work was funded by National Science Foundation grant EAR 1609027 to E. M. H. and L. K. C. The Alaskan Peatland Experiment is supported by NSF DEB (LTREB) 1354370 to E. S. K. NGEE Arctic is funded through the Department of Energy Office of Science, Biological and Environmental Research (BER) Program (ERPK757). This research used resources of the Advanced Photon Source, a U.S. Department of Energy (DOE) Office of Science User Facility operated for the DOE Office of Science by Argonne National Laboratory under contract DE-AC02-06CH11357. X-ray absorption spectra were collected at sector 12BM with support from Benjamin Reinhart. Mössbauer data were collected through support of NSF grants DEB-1457761 and EAR-1451508 to A. T. The authors declare no conflict of interest. All data generated or analyzed during this study are included with the published article and the supporting information files.

References

Amacher, M. C., Henderson, R. E., Breithaupt, M. D., Seale, C. L., & LaBauve, J. M. (1990). Unbuffered and buffered salt methods for exchangeable cations and effective cation-exchange capacity. *Soil Science Society of America Journal*, *54*(4), 1036–1042. https://doi.org/10.2136/sssaj1990.03615995005400040018x

Avis, C. A., Weaver, A. J., & Meissner, K. J. (2011). Reduction in areal extent of high-latitude wetlands in response to permafrost thaw. *Nature Geoscience*, *4*(7), 444–448. https://doi.org/10.1038/ngeo1160

Bache, B. W., & Williams, E. G. (1971). A phosphate sorption index for soils. *Journal of Soil Science*, *22*(3), 289–301. https://doi.org/10.1111/j.1365-2389.1971.tb01617.x

Bekryaev, R. V., Polyakov, I. V., & Alexeev, V. A. (2010). Role of polar amplification in long-term surface air temperature variations and modern arctic warming. *Journal of Climate*, *23*(14), 3888–3906. https://doi.org/10.1175/2010JCLI3297.1

Bhattacharyya, A., Schmidt, M. P., Stavitski, E., & Martínez, C. E. (2018). Iron speciation in peats: Chemical and spectroscopic evidence for the co-occurrence of ferric and ferrous iron in organic complexes and mineral precipitates. *Organic Geochemistry*, *115*, 124–137. https://doi.org/10.1016/j.orggeochem.2017.10.012

Bockheim, J. G., Hinkel, K. M., & Nelson, F. E. (2003). Predicting carbon storage in tundra soils of Arctic Alaska. *Soil Science Society of America Journal*, *67*(3), 948. https://doi.org/10.2136/sssaj2003.0948

Bridgham, S. D., Updegraff, K., & Pastor, J. (1998). Carbon, nitrogen, and phosphorus mineralization in northern wetlands. *Ecology*, *79*(5), 1545–1561. https://doi.org/10.1890/0012-9658(1998)079[1545:CNAPMI]2.0.CO;2

Bring, A., Fedorova, I., Dibike, Y., Hinzman, L., Mård, J., Mernild, S. H., et al. (2016). Arctic terrestrial hydrology: A synthesis of processes, regional effects, and research challenges. *Journal of Geophysical Research: Biogeosciences*, *121*, 621–649. https://doi.org/10.1002/2015JG003131

Chapin, F. S., Barsdate, R., & Barel, D. (1978). Phosphorus cycling in Alaksan coastal tundra: A hypothesis for the regulation of nutrient cycling. *Oikos*, *31*(2), 189–199. https://doi.org/10.2307/3543562

Chapin, F. S. III, Shaver, G. R., Giblin, A. E., Nadelhoffer, K. J., & Laundre, J. A. (1995). Responses of Arctic tundra to experimental and observed changes in climate. *Ecology*, *76*(3), 694–711. https://doi.org/10.2307/1939337

Chen, C., Meile, C., Wilmoth, J. L., Barcellos, D., & Thompson, A. (2018). Influence of pO_2 on iron redox cycling and anaerobic organic carbon mineralization in a humid tropical forest soil. *Environmental Science & Technology*, *52*, 7709–7719. https://doi.org/10.1021/acs.est.8b01368

Chen, C., & Thompson, A. (2018). Ferrous iron oxidation under varying pO_2 levels: The effect of Fe (III)/Al (III) oxide minerals and organic matter. *Environmental Science & Technology*, *52*(2), 597–606. https://doi.org/10.1021/acs.est.7b05102

Cherry, J. E., Dery, S. J., Cheng, Y., Stieglitz, M., Jacobs, A. S., & Pan, F. (2014). Climate and hydrometerology of the Toolik Lake region and the Kuparuk River Basin: Past, present, and future. In J. E. Hobbie, & G. W. Kling (Eds.), *Alaska's changing Arctic* (pp. 21–60). New York, NY: Oxford University Press. https://doi.org/10.1093/acprof:osobl/9780199860401.003.0002

Darke, A. K., & Walbridge, M. R. (2000). Al and Fe biogeochemistry in a floodplain forest: Implications for P retention. *Biogeochemistry*, *51*(1), 1–32. https://doi.org/10.1023/A:1006302600347

Emerson, D., Scott, J. J., Benes, J., & Bowden, W. B. (2015). Microbial iron oxidation in the Arctic tundra and the implications for biogeochemical cycling. *Applied and Environmental Microbiology*, *81*(23), 8066–8075. https://doi.org/10.1128/AEM.02832-15

Fiedler, S., Wagner, D., Kutzbach, L., & Pfeiffer, E.-M. (2004). Element redistribution along hydraulic and redox gradients of low-centered polygons, Lena Delta, northern Siberia. *Soil Science Society of America Journal*, *68*(3), 1002. https://doi.org/10.2136/sssaj2004.1002

Froelich, P. N. (1988). Kinetic control of dissolved phosphate in natural rivers and estuaries: A primer on the phosphate buffering mechanism. *Limnology and Oceanography*, *33*(4), 649–668.

Gardner, W. H. (1986). Water content. In *Methods of soil analysis: Part 1. Physical and mineralogical methods* (pp. 493–544). Madison WI: Soil Science Society of America, American Society of Agronomy.

Giblin, A. E., Nadelhoffer, K. J., Shaver, G. R., Laundre, J. A., & McKerrow, A. J. (1991). Biogeochemical diversity along a riverside toposequence in Arctic Alaska. *Ecological Monographs*, *61*(4), 415–435. https://doi.org/10.2307/2937049

Giesler, R., Andersson, T., Lövgren, L., & Persson, P. (2005). Phosphate sorption in aluminum- and iron-rich humus soils. *Soil Science Society of America Journal*, *69*(4), 77–86. https://doi.org/10.2136/sssaj2005.0077

Hall, S. J., Berhe, A. A., & Thompson, A. (2018). Order from disorder: Do soil organic matter composition and turnover co-vary with iron phase crystallinity? *Biogeochemistry*, *140*(1), 93–110. https://doi.org/10.1007/s10533-018-0476-4

Hanson, P. J., Riggs, J. S., Robert Nettles, W., Phillips, J. R., Krassovski, M. B., Hook, L. A., et al. (2017). Attaining whole-ecosystem warming using air and deep-soil heating methods with an elevated CO_2 atmosphere. *Biogeosciences*, *14*(4), 861–883. https://doi.org/10.5194/bg-14-861-2017

Harms, T. K., & Ludwig, S. M. (2016). Retention and removal of nitrogen and phosphorus in saturated soils of arctic hillslopes. *Biogeochemistry*, *127*(2–3), 291–304. https://doi.org/10.1007/s10533-016-0181-0

Henderson, R., Kabengi, N., Mantripragada, N., Cabrera, M., Hassan, S., & Thompson, A. (2012). Anoxia-induced release of colloid- and nanoparticle-bound phosphorus in grassland soils. *Environmental Science & Technology*, *46*(21), 11,727–11,734. https://doi.org/10.1021/es302395r

Herndon, E., AlBashaireh, A., Singer, D., Roy Chowdhury, T., Gu, B., & Graham, D. (2017). Influence of iron redox cycling on organo-mineral associations in Arctic tundra soil. *Geochimica et Cosmochimica Acta*, *207*, 210–231. https://doi.org/10.1016/j.gca.2017.02.034

Herndon, E. M., Yang, Z., Bargar, J., Janot, N., Regier, T. Z., Graham, D. E., Wullschleger, S. D., et al. (2015). Geochemical drivers of organic matter decomposition in arctic tundra soils. *Biogeochemistry*, *126*(3), 397–414. https://doi.org/10.1007/s10533-015-0165-5

Hill, B. H., Elonen, C. M., Jicha, T. M., Kolka, R. K., Lehto, L. L. P., Sebestyen, S. D., & Seifert-Monson, L. R. (2014). Ecoenzymatic stoichiometry and microbial processing of organic matter in northern bogs and fens reveals a common P-limitation between peatland types. *Biogeochemistry*, *120*(1–3), 203–224. https://doi.org/10.1007/s10533-014-9991-0

Hinzman, L., Viereck, L., Adams, P. C., Romanovsky, V., & Yoshikawa, K. (2006). Climate and permafrost dynamics of the Alaskan boreal forest. In F. S. Chapin (Ed.), *Alaska's changing boreal forest* (pp. 39–61). Oxford University Press.

Hinzman, L. D., Deal, C. J., Mcguire, A. D., Mernild, S. H., Polyakov, I. V., & Walsh, J. E. (2013). Trajectory of the Arctic as an integrated system. *Ecological Applications*, *23*(8), 1837–1868. https://doi.org/10.1890/11-1498.1

Hobara, S., Kushida, K., Kim, Y., Koba, K., Lee, B. Y., & Ae, N. (2016). Relationships among pH, minerals, and carbon in soils from tundra to boreal forest across Alaska. *Ecosystems*, *19*(6), 1092–1103.

Hubbard, S. S., Gangodagamage, C., Dafflon, B., Wainwright, H., Peterson, J., Gusmeroli, A., et al. (2013). Quantifying and relating land-surface and subsurface variability in permafrost environments using LiDAR and surface geophysical datasets. *Hydrogeology Journal*, *21*(1), 149–169. https://doi.org/10.1007/s10040-012-0939-y

Kane, E. S., Turetsky, M. R., Harden, J. W., McGuire, A. D., & Waddington, J. M. (2010). Seasonal ice and hydrologic controls on dissolved organic carbon and nitrogen concentrations in a boreal-rich fen. *Journal of Geophysical Research*, *115*, G04012. https://doi.org/10.1029/2010JG001366

Karlsson, T., & Persson, P. (2010). Coordination chemistry and hydrolysis of Fe (III) in a peat humic acid studied by X-ray absorption spectroscopy. *Geochimica et Cosmochimica Acta*, *74*(1), 30–40. https://doi.org/10.1016/j.gca.2009.09.023

Karlsson, T., Persson, P., Skyllberg, U., Mörth, C.-M., & Giesler, R. (2008). Characterization of iron (III) in organic soils using extended X-ray absorption fine structure spectroscopy. *Environmental Science & Technology*, *42*(15), 5449–5454. https://doi.org/10.1021/es800322j

Kinsman-Costello, L. E., O'Brien, J., & Hamilton, S. K. (2014). Re-flooding a historically drained wetland leads to rapid sediment phosphorus release. *Ecosystems*, *17*(4), 641–656. https://doi.org/10.1007/s10021-014-9748-6

Kizewski, F. R., Boyle, P., Hesterberg, D., & Martin, J. D. (2010). Mixed anion (phosphate/oxalate) bonding to iron (III) materials. *Journal of the American Chemical Society*, *132*(7), 2301–2308. https://doi.org/10.1021/ja908807b

Koven, C. D., Ringeval, B., Friedlingstein, P., Ciais, P., Cadule, P., Khvorostyanov, D., et al. (2011). Permafrost carbon-climate feedbacks accelerate global warming. *Proceedings of the National Academy of Sciences of the United States of America*, *108*(36), 14,769–14,774. https://doi.org/10.1073/pnas.1103910108

Kraft, S., Stümpel, J., Becker, P., & Kuetgens, U. (1996). High resolution X-ray absorption spectroscopy with absolute energy calibration for the determination of absorption edge energies. *Review of Scientific Instruments*, *67*(3), 681–687. https://doi.org/10.1063/1.1146657

Lalonde, A. E., Rancourt, D. G., & Ping, J. Y. (1998). Accuracy of ferric/ferrous determinations in micas: A comparison of Mössbauer spectroscopy and the Pratt and Wilson wet-chemical methods. *Hyperfine Interactions*, *117*(1/4), 175–204. https://doi.org/10.1023/A:1012607813487

Lin, Y., Bhattacharyya, A., Campbell, A. N., Nico, P. S., Pett-Ridge, J., & Silver, W. L. (2018). Phosphorus fractionation responds to dynamic redox conditions in a humid tropical forest soil. *Journal of Geophysical Research: Biogeosciences*, *123*, 3016–3027. https://doi.org/10.1029/2018JG004420

Lipson, D. A., Jha, M., Raab, T. K., & Oechel, W. C. (2010). Reduction of iron (III) and humic substances plays a major role in anaerobic respiration in an Arctic peat soil. *Journal of Geophysical Research*, *115*, G00I06. https://doi.org/10.1029/2009JG001147

Lipson, D. A., Zona, D., Raab, T. K., Bozzolo, F., Mauritz, M., & Oechel, W. C. (2012). Water-table height and microtopography control biogeochemical cycling in an Arctic coastal tundra ecosystem. *Biogeosciences*, *9*(1), 577–591. https://doi.org/10.5194/bg-9-577-2012

Mack, M. C., Schuur, E. A. G., Bret-Harte, M. S., Shaver, G. R., & Chapin, F. S. (2004). Ecosystem carbon storage in arctic tundra reduced by long-term nutrient fertilization. *Nature*, *431*(7007), 440–443. https://doi.org/10.1038/nature02887

McGuire, A. D., Genet, H., Lyu, Z., Pastick, N. J., Stackpoole, S. M., Birdsey, R., et al. (2018). Assessing historical and projected carbon balance of Alaska: A synthesis of results and policy/management implications. *Ecological Applications*, *28*(6), 1396–1412. https://doi.org/10.1002/eap.1768

Nadelhoffer, K. J., Giblin, A. E., Shaver, G. R., & Laundre, J. A. (1991). Effects of temperature and substrate quality on element mineralization in six Arctic soils. *Ecology*, *72*(1), 242–253. https://doi.org/10.2307/1938918

Nelson, D. W., & Sommers, L. E. (1996). Total carbon, organic carbon, and organic matter. In D. Sparks et al. (Eds.), *Methods of soil analysis. Part 3. Chemical Methods* (pp. 961–1010).

Newman, B. D., Throckmorton, H. M., Graham, D. E., Gu, B., Hubbard, S. S., Liang, L., et al. (2015). Microtopographic and depth controls on active layer chemistry in Arctic polygonal ground. *Geophysical Research Letters*, *42*. https://doi.org/10.1002/2014GL062804, 1808–1817.

Newville, M. (2014). Fundamentals of XAFS. *Reviews in Mineralogy and Geochemistry*, *78*(1), 33–74. https://doi.org/10.2138/rmg.2014.78.2

O'Day, P. A., Rivera, N., Root, R., & Carroll, S. A. (2004). X-ray absorption spectroscopic study of Fe reference compounds for the analysis of natural sediments. *American Mineralogist*, *89*(4), 572–585. https://doi.org/10.2138/am-2004-0412

Oechel, W. C., Hastings, S. J., Vourlrtis, G., Jenkins, M., Riechers, G., & Grulke, N. (1993). Recent change of Arctic tundra ecosystems from a net carbon dioxide sink to a source. *Nature*, *361*(6412), 520–523. https://doi.org/10.1038/361520a0

Olefeldt, D., Euskirchen, E. S., Harden, J., Kane, E., McGuire, A. D., Waldrop, M. P., & Turetsky, M. R. (2017). A decade of boreal rich fen greenhouse gas fluxes in response to natural and experimental water table variability. *Global Change Biology*, *23*(6), 2428–2440. https://doi.org/10.1111/gcb.13612

Page, S. E., Kling, G. W., Sander, M., Harrold, K. H., Robert, J., Mcneill, K., & Cory, R. M. (2013). Dark production of hydroxyl radical in arctic soil and surface waters. *Environmental Science and Technology*, *47*(22), 12,860–12,867. https://doi.org/10.1021/es4033265

Paludan, C., & Jensen, H. S. (1995). Sequential extraction of phosphorus in freshwater wetland and lake sediment: Significance of humic acids. *Wetlands*, *15*(4), 365–373. https://doi.org/10.1007/BF03160891

Poulton, S. W., & Canfield, D. E. (2005). Development of a sequential extraction procedure for iron: Implications for iron partitioning in continentally derived particulates. *Chemical Geology*, *214*(3–4), 209–221. https://doi.org/10.1016/j.chemgeo.2004.09.003

Racine, C. H., & Walters, J. C. (1994). Groundwater-discharge fens in the Tanana Lowlands, Interior Alaska, U.S.A. *Arctic and Alpine Research*, *26*(4), 418–426. https://doi.org/10.2307/1551804

Rancourt, D. G. (1998). Mössbauer spectroscopy in clay science. *Hyperfine Interactions*, *117*(1/4), 3–38. https://doi.org/10.1023/A:1012651628508

Rancourt, D. G., & Ping, J. Y. (1991). Voigt-based methods for arbitrary-shape static hyperfine parameter distributions in Mössbauer spectroscopy. *Nuclear Instruments and Methods in Physics Research Section B: Beam Interactions with Materials and Atoms*, *58*(1), 85–97. https://doi.org/10.1016/0168-583X(91)95681-3

Ravel, B., & Newville, M. (2005). ATHENA, ARTEMIS, HEPHAESTUS: Data analysis for X-ray absorption spectroscopy using IFEFFIT. *Journal of Synchrotron Radiation*, *12*(4), 537–541. https://doi.org/10.1107/S0909049505012719

Reitzel, K., Ahlgren, J., Gogoll, A., Jensen, H. S., & Rydin, E. (2006). Characterization of phosphorus in sequential extracts from lake sediments using ^{31} P nuclear magnetic resonance spectroscopy. *Canadian Journal of Fisheries and Aquatic Sciences*, *63*(8), 1686–1699. https://doi.org/10.1139/f06-070

Richardson, M. C., Mitchell, C. P. J., Branfireun, B. A., & Kolka, R. K. (2010). Analysis of airborne LiDAR surveys to quantify the characteristic morphologies of northern forested wetlands. *Journal of Geophysical Research*, *115*, G03005. https://doi.org/10.1029/2009jg000972

Riedel, T., Zak, D., Biester, H., & Dittmar, T. (2013). Iron traps terrestrially derived dissolved organic matter at redox interfaces. *Proceedings of the National Academy of Sciences*, *110*(25), 10,101–10,105. https://doi.org/10.1073/pnas.1221487110

Roy Chowdhury, T., Herndon, E. M., Phelps, T. J., Elias, D. A., Gu, B., Liang, L., et al. (2015). Stoichiometry and temperature sensitivity of methanogenesis and CO_2 production from saturated polygonal tundra in Barrow, Alaska. *Global Change Biology*, *21*(2), 722–737. https://doi.org/10.1111/gcb.12762

Schaefer, K., Lantuit, H., Romanovsky, V. E., Schuur, E. A. G., & Witt, R. (2014). The impact of the permafrost carbon feedback on global climate. *Environmental Research Letters*, *9*(8). https://doi.org/10.1088/1748-9326/9/8/085003

Schuur, E. A. G., Vogel, J. G., Crummer, K. G., Lee, H., Sickman, J. O., & Osterkamp, T. E. (2009). The effect of permafrost thaw on old carbon release and net carbon exchange from tundra. *Nature*, *459*(7246), 556–559. https://doi.org/10.1038/nature08031

Schwertmann, U., & Cornell, R. M. (2008). *Iron oxides in the laboratory* (2nd ed.). Weinheim (Federal Republic of Germany): Wiley-VCH.

Sebestyen, S. D., Dorrance, C., Olson, D. M., Verry, E. S., Kolka, R. K., Elling, A. E., & Kyllander, R. (2011). Long-term monitoring sites and trends at the Marcell Experimental Forest. In R. Kolka, S. Sebestyen, E. S. Verry, & K. Brooks (Eds.), *Peatland biogeochemistry and watershed hydrology at the Marcell Experimental Forest* (pp. 15–71). Taylor Francis Group: CRC Press. https://doi.org/10.1201/b10708-3

Shaver, G. R., & Chapin, F. S. III (1995). Long-term responses to factorial, NPK fertilizer treatment by Alaskan wet and moist tundra sedge species. *Ecography*, *18*(3), 259–275. https://doi.org/10.1111/j.1600-0587.1995.tb00129.x

Shaver, G. R., Johnson, L. C., Cades, D. H., Murray, G., Laundre, J. A., Nadelhoffer, K. J., & Giblin, A. E. (1998). Biomass and CO_2 flux in wet sedge tundras: Responses to nutrients, temperature, and light. *Ecological Monographs*, *68*(1), 75–97.

Shaver, G. R., Laundre, J. A., Bret-Harte, M. S., Chapin, F. S., Mercado-Dıaz, J. A., Giblin, A. E., et al. (2014). Terrestrial ecosystems at Toolik Lake, Alaska. In J. E. Hobbie, & G. W. Kling (Eds.), *Alaska's changing Arctic: Ecological consequences for tundra, streams, and lakes* (pp. 90–142). New York, NY: Oxford University Press.

Siregar, A., Kleber, M., Mikutta, R., & Jahn, R. (2005). Sodium hypochlorite oxidation reduces soil organic matter concentrations without affecting inorganic soil constituents. *European Journal of Soil Science*, *56*(4), 481–490. https://doi.org/10.1111/j.1365-2389.2004.00680.x

Stocker, T., Qin, D., Plattner, G.-K., Tignor, M., Allen, S., Boschung, J., et al. (Eds) (2013). Climate Change 2013: The physical science basis. In *Contribution of Working Group I to the Fifth Assessment Report of the Intergovernmental Panel on Climate Change* (1535 pp.). Cambridge, United Kingdom; New York, NY, USA: Cambridge University Press.

Strauss, R., Brümmer, G. W., & Barrow, N. J. (1997). Effects of crystallinity of goethite: II. Rates of sorption and desorption of phosphate. *European Journal of Soil Science*, *48*(1), 101–114. https://doi.org/10.1111/j.1365-2389.1997.tb00189.x

Street, L. E., Mielke, N., & Woodin, S. J. (2017). Phosphorus availability determines the response of tundra ecosystem carbon stocks to nitrogen enrichment. *Ecosystems*, *21*(6), 1155–1167. https://doi.org/10.1007/s10021-017-0209-x

Sundman, A., Karlsson, T., Laudon, H., & Persson, P. (2014). XAS study of iron speciation in soils and waters from a boreal catchment. *Chemical Geology*, *364*, 93–102. https://doi.org/10.1016/j.chemgeo.2013.11.023

Swindles, G. T., Morris, P. J., Mullan, D., Watson, E. J., Turner, T. E., Roland, T. P., et al. (2016). The long-term fate of permafrost peatlands under rapid climate warming. *Scientific Reports*, *5*(1), 17,951. https://doi.org/10.1038/srep17951

Trusiak, A., Treibergs, L. A., Kling, G. W., & Cory, R. M. (2018). The role of iron and reactive oxygen species in the production of CO_2 in arctic soil waters. *Geochimica et Cosmochimica Acta*, *224*, 80–95. https://doi.org/10.1016/j.gca.2017.12.022

Turetsky, M. R., Treat, C. C., Waldrop, M. P., Waddington, J. M., Harden, J. W., & McGuire, A. D. (2008). Short-term response of methane fluxes and methanogen activity to water table and soil warming manipulations in an Alaskan peatland. *Journal of Geophysical Research*, *113*, G00A10. https://doi.org/10.1029/2007JG000496

Verry, E. S., Brooks, K. N., Nichols, D. S., Ferris, D. R., & Sebestyen, S. D. (2011). Watershed hydrology. In R. Kolka, S. Sebestyen, E. S. Verry, & K. Brooks (Eds.), *Peatland biogeochemistry and watershed hydrology at the Marcell Experimental Forest* (pp. 193–212). Boca Raton, FL: CRC Press. https://doi.org/10.1201/b10708-8

Viereck, L. K., VanCleve, K., Adams, P. C., & Schlentner, R. E. (1993). Climate of the Tanana River floodplain near Fairbanks, Alaska. *Canadian Journal of Forest Research*, *23*(5), 899–913. https://doi.org/10.1139/x93-118

Vincent, A. G., Sundqvist, M. K., Wardle, D. A., & Giesler, R. (2014). Bioavailable soil phosphorus decreases with increasing elevation in a subarctic tundra landscape. *PLoS One*, *9*(3), e92942–e92911. https://doi.org/10.1371/journal.pone.0092942

Vitousek, P. M., Porder, S., Houlton, B. Z., & Chadwick, O. a. (2010). Terrestrial phosphorus limitation: Mechanisms, implications, and nitrogen—Phosphorus interactions. *Ecological Applications*, *20*(1), 5–15. https://doi.org/10.1890/08-0127.1

Walbridge, M. R., & Navaratnam, J. A. (2006). Phosphorus in boreal peatlands. In R. K. Wieder & D. H. Vitt (Eds.), *Boreal peatland ecosystems* (pp. 231–258). Berlin, Heidelberg: Springer. https://doi.org/10.1007/978-3-540-31913-9_11

Walker, T. W., & Syers, J. K. (1976). The fate of phosphorus during pedogenesis. *Geoderma*, *15*(1), 1–19. https://doi.org/10.1016/0016-7061(76)90066-5

Wang, X., Liu, F., Tan, W., Li, W., Feng, X., & Sparks, D. L. (2013). Characteristics of phosphate adsorption-desorption onto ferrihydrite. *Soil Science*, *178*(1), 1–11. https://doi.org/10.1097/SS.0b013e31828683f8

Weintraub, M. N. (2011). Biological phosphorus cycling in Arctic and Alpine soils. In E. Bünemann, A. Oberson, & E. Frossard (Eds.), *Phosphorus in action* (Vol. 26, pp. 295–316). Berlin Heidelberg: Springer. https://doi.org/10.1007/978-3-642-15271-9

Weintraub, M. N., & Schimel, J. P. (2005). The seasonal dynamics of amino acids and other nutrients in Alaskan Arctic tundra soils. *Biogeochemistry*, *73*(2), 359–380. https://doi.org/10.1007/sl0533-004-0363-z

Whittinghill, K. A., & Hobbie, S. E. (2011). Effects of landscape age on soil organic matter processing in northern Alaska. *Soil Science Society of America Journal*, *75*(3), 907. https://doi.org/10.2136/sssaj2010.0318

Wieder, W. R., Cleveland, C. C., Smith, W. K., & Todd-Brown, K. (2015). Future productivity and carbon storage limited by terrestrial nutrient availability. *Nature Geoscience*, *8*(6), 441–444. https://doi.org/10.1038/ngeo2413

Yoshikawa, K., & Hinzman, L. D. (2003). Shrinking thermokarst ponds and groundwater dynamics in discontinuous permafrost near Council, Alaska. *Permafrost and Periglacial Processes*, *14*(2), 151–160. https://doi.org/10.1002/ppp.451

Zak, D., Gelbrecht, J., & Steinberg, C. E. W. (2004). Phosphorus retention at the redox interface of peatlands adjacent to surface waters in Northeast Germany. *Biogeochemistry*, *70*(3), 357–368. https://doi.org/10.1007/s10533-003-0895-7

Zona, D., Lipson, D. A., Zulueta, R. C., Oberbauer, S. F., & Oechel, W. C. (2011). Microtopographic controls on ecosystem functioning in the Arctic Coastal Plain. *Journal of Geophysical Research*, *116*, G00I08. https://doi.org/10.1029/2009JG001241